Journal Name

ARTICLE TYPE

Cite this: DOI: 10.1039/xxxxxxxxxx

Clustering and phase behaviour of attractive active particles with hydrodynamics†

Ricard Matas Navarro,[a] and Suzanne Fielding*[a]

Received Date
Accepted Date

DOI: 10.1039/xxxxxxxxxx

www.rsc.org/journalname

We simulate clustering, phase separation and hexatic ordering in a monolayered suspension of active squirming disks subject to an attractive Lennard-Jones-like pairwise interaction potential, taking hydrodynamic interactions between the particles fully into account. By comparing the hydrodynamic case with counterpart simulations for passive and active Brownian particles, we elucidate the relative roles of self-propulsion, interparticle attraction, and hydrodynamic interactions in determining clustering and phase behaviour. Even in the presence of an attractive potential, we find that hydrodynamic interactions strongly suppress the motility induced phase separation that might a priori have been expected in a highly active suspension. Instead, we find only a weak tendency for the particles to form stringlike clusters in this regime. At lower activities we demonstrate phase behaviour that is broadly equivalent to that of the counterpart passive system at low temperatures, characterized by regimes of gas-liquid, gas-solid and liquid-solid phase coexistence. In this way, we suggest that a dimensionless quantity representing the level of activity relative to the strength of attraction plays the role of something like an effective non-equilibrium temperature, counterpart to the (dimensionless) true thermodynamic temperature in the passive system. However there are also some important differences from the equilibrium case, most notably with regards the degree of hexatic ordering, which we discuss carefully.

1 Introduction

Active matter comprises internal mesoscopic subunits that collectively drive the system far from thermal equilibrium by each individually converting internal energy into mechanical work. In a biological context, examples include crosslinked filaments activated by molecular motors in the cell cytoskeleton[1], cells collectively organised in living tissues[2], suspensions of motile microorganisms[3,4], shoals of fish and flocks of birds[5]. Synthetic examples include vibrated granular monolayers[6–8] and suspensions of phoretic colloidal particles[9–11]. As has been well documented in recent reviews[12–14], active systems display a host of exotic emergent effects including swarming, pattern formation, giant number fluctuations and nonequilibrium ordering. Among these, this paper focuses in particular on the phenomena of aggregation and phase separation in active suspensions.

In the literature, (at least) two mechanisms have been put forward to suggest that activity should generically lead to aggregation. The first[15–20] operates in systems of active particles that are elongated and so have an intrinsic (steric) tendency to align with each other. An activity-mediated coupling between these orientational modes and fluctuations in the local number density then provides a mechanism for giant number fluctuations and phase separation. The standard deviation ΔN of particle number in a subsystem with a mean number of particles N then scales as N^a, with $a > 1/2$.

The second mechanism[21–23] does not rely on steric orientational effects and operates even in systems of spherically symmetric particles. It was put forward originally in the context of certain species of bacteria that obey simple "run-and-tumble" dynamics, in which each particle (at least when in isolation from any other particle) swims in straight lines at constant speed between intermittent tumbling events in which it suddenly changes swim direction. A positive feedback loop then arises in which the particles (a) accumulate in regions where they move more slowly and (b) further slow down in regions where they are impeded by crowding from other particles. This renders an initially uniform suspension unstable to "motility induced phase separation" (MIPS)[21,22]. Following its prediction, MIPS was indeed subsequently observed in simulations of spherical (or disklike) active particles[24–27].

These simulations however discard hydrodynamic interactions between the particles, which are of widespread importance in active systems. Motivated by this, in Ref.[28] we simulated a suspen-

[a] Department of Physics, University of Durham, Science Laboratories, South Road, DH1 3LE, Durham, United Kingdom. E-mail: suzanne.fielding@durham.ac.uk

† Electronic Supplementary Information (ESI) available: movies of "living crystal" squirmer suspensions. See DOI: 10.1039/b000000x/

sion of active squirming disks with full hydrodynamics. In doing so we showed that hydrodynamic interactions in fact strongly suppress MIPS, with the predicted phase separation replaced by only a very weak stringlike clustering.

We interpreted this suppression in terms of the breakdown of a mean-field assumption contained in the (a)-(b) feedback mechanism outlined above: if a particle is to experience a slowing of its run by crowding from other particles (part (b)), it must suffer many collisions during any such run. This assumption breaks down in the case of hydrodynamic squirmers, because whenever two squirmers scatter off each other hydrodynamically they each suffer an $O(1)$ change in swim direction[29]. To support this interpretation, we further demonstrated suppression of MIPS even without hydrodynamics, in active Brownian particles in any regime where the time for the decorrelation of swim direction fails to comfortably exceed the time between particle collisions. The importance of rotational and translational timescales in determining phase separation was also discussed in Refs.[30,31].

Nonetheless, strong aggregation effects have been widely observed experimentally in active suspensions such as monolayered light-activated colloidal surfers[32] and phoretic colloidal Janus particles[9–11]. Conversely, however, many bacterial suspensions show pronounced coherent structures in their velocity field without strong spatial inhomogeneities in concentration[33–35], although aggregation has been studied in suspensions of bacteria (with and without active flagellae) subject to an attractive depletion interaction[36–38].

In many of these experimental systems, the presence of a slight attractive potential between the particles cannot be ruled out. In contrast, the simulation study of Ref.[28] concerned particles that, besides hydrodynamic effects, interact only via a purely repulsive potential that onsets steeply at particle-particle contact. The original predictions of MIPS likewise concerned purely repulsive hard particles[21,22]. A key open question, therefore, is whether the presence of an attractive contribution to the inter-particle potential might restore a tendency for active suspensions to phase separate, even in the presence of hydrodynamics.

As noted above, the phase behaviour of active particles has been extensively studied in the absence of hydrodynamic interactions by means of Brownian dynamics simulations, both without[24–26,30,31,39–45] and with[46–48] attractive interactions between the particles. In particular, Ref.[47] reported attraction-dominated phase separation at low activity, with a crossover to MIPS at higher levels of activity. However these existing studies of attractive active systems again neglect hydrodynamic interactions. Given the strong effect of hydrodynamics on the phase behaviour of purely repulsive active suspensions[28], an important outstanding problem is to elucidate the phase behaviour of attractive active suspensions with hydrodynamics.

With that motivation in mind, in this work we simulate a suspension of active squirming particles[49,50] with an attractive Lennard-Jones component to the potential of interaction between them. Hydrodynamic interactions are taken fully into account using the simulation method of Ref.[28], which allows for short range lubrication, long range (power law) propagators, and indeed hydrodynamic effects on all lengthscales in between. The method moreover gives access to the full range of packing fractions from dilute to close packed, thereby allowing a comprehensive study of phase behaviour. In these hydrodynamic simulations we neglect Brownian motion, considering the limit of purely athermal dynamics that is relevant to many active systems, such as bacterial suspensions. We return below to justify this neglect more fully by commenting on the likely effect of a non-zero temperature.

To understand the effects of activity in the face of this attractive component to the interaction potential, we define a dimensionless parameter that quantifies the strength of swimming compared to the strength of the attractive interaction. For small values of this parameter (low activity), we shall find phase behaviour that is dominated by this attractive interaction, as might be expected intuitively. In particular, we find regimes of phase coexistence (gas-solid, gas-liquid, liquid-solid, *etc.*) that closely resemble those of passive, thermalised LJ particles. In this sense, the scaled activity parameter for the active system might be viewed as a dimensionless effective temperature that plays a role somewhat analogous to the true dimensionless temperature in the counterpart passive LJ system. There are however some important differences between the attraction-dominated phase separation that we report here in the active system and its equilibrium counterpart, most notably with regards the degree of crystalline ordering.

In contrast, for high levels of activity we find phase behaviour that is relatively unaffected by the LJ attraction. This is also consistent with intuition, because strongly swimming particles are expected to be much less affected by the attractive interaction. Indeed in this regime we find only a weak tendency for stringlike clustering. We give evidence to support the interpretation that this is again the signature of a nearby MIPS that has been narrowly avoided by the hydrodynamic suppression mechanism[28] outlined above for purely repulsive particles.

In between these two limiting regimes - attraction-dominated phase separation at low activity, and stringlike clustering at high activity - we find a slow crossover region in which the two effects merge, with a degree of particle clustering that is set by the packing fraction and the dimensionless activity parameter.

Alongside the attractive Lennard Jones contribution to the interaction potential, a steep repulsive interaction is also present that diverges at particle contact, *i.e.,* at a particle separation $r \to 2R^+$, where R is the bare (hydrodynamic) radius of the squirmers. We therefore expect much stronger excluded volume effects than for the LJ potential that is conventionally used in the literature, which diverges only at full overlap $r \to 0^+$. In view of this, as a warmup to our hydrodynamic simulations we shall first map out the phase behaviour of both passive and active Brownian particles with this modified LJ potential, in the absence of hydrodynamics. This will then provide a benchmark against which the results of the hydrodynamic study can be properly compared.

Because of the heavy computational cost of simulating dense suspensions with full hydrodynamics, we have only been able to access a relatively small number of particles in each run, typically $N = 242$. Phase diagrams will therefore be elucidated in qualitative outline only, most obviously near any critical point. Indeed this provides an additional motivation for first simulating passive and active Brownian particles, in order to learn what features

of phase behaviour we can realistically expect to capture with this small $N = 242$. Accordingly, although we could in principle achieve much larger $N = 10^5$ or even $N = 10^6$ in the Brownian simulations, we use $N = 242$ here too, to provide a true comparison with the hydrodynamic results. While this small N is clearly a limitation, it is worth remarking that some of the experiments reporting clustering of artificial swimmers also involve a relatively small number of particles. We note also that the first simulations to map out the phase behaviour of passive Lennard Jonesium used a similarly small N[51–53].

The paper is organized as as follows. In Sec. 2 we describe the Brownian and hydrodynamic models to be studied, along with the simulation methods used. Sec. 3 summarizes the model parameters, our choice of units, and the principal adimensional quantities to be explored in the simulations. In Sec. 4 we discuss the initial condition used in the simulations, before in Sec. 5 defining the statistical quantities that we shall measure during the runs. In Sec. 6 we present our results for passive Brownian particles, active Brownian particles and hydrodynamic squirmers in turn. Sec. 7 contains our conclusions.

2 Models

In this section we introduce the three models to be studied in the remainder of the manuscript. We start by defining the modified Lennard-Jones interaction potential that is common to all three models. We then define the dynamical rules of the three models separately: passive Brownian particles (PBP), active Brownian particles (ABP) and hydrodynamic squirmers (HS or simply squirmers). Note that each model has its own set of dynamical rules, but all are subject to the same modified Lennard-Jones potential.

For all three models we consider a two dimensional (2D) system comprising N disks in a square box of side L with periodic boundary conditions. Each particle has a bare radius R (bare in a sense to be defined below), implying a bare area fraction $\phi_r = N\pi R^2/L^2$.

2.1 Potential

The particles experience pairwise Lennard-Jones interactions governed by the potential

$$V_{\rm LJ}(r) = 4\varepsilon_{\rm LJ}\left[\left(\frac{\sigma_{\rm LJ}}{r}\right)^{12} - \left(\frac{\sigma_{\rm LJ}}{r}\right)^{6}\right], \qquad (1)$$

which gives short-ranged repulsion for particle separations $r < 2^{1/6}\sigma_{\rm LJ}$, and long-ranged attraction for particle separations $r > 2^{1/6}\sigma_{\rm LJ}$. See the dotted line in Fig. 1. Setting $\sigma_{\rm LJ} = 2R$ then sets the minimum of $V_{\rm LJ}$ to be located at $r = 2^{7/6}R$.

As we shall describe in more detail below, the hydrodynamically squirming disks propel themselves by effecting a tangential velocity round their edges, at a hydrodynamic radius R from the particle centres. Given the hydrodynamic interactions that we shall also describe, short range lubrication effects then in principle disallow any particle overlaps in which particles approach each other to a separation $r < 2R$. However the inevitably finite discretisation of time and space in the simulation can in practice result in occasional overlaps. To prevent these we follow standard practice in the literature and include an additional short ranged steep repulsive contribution

$$V_{\rm h}(r) = \varepsilon_{\rm h}\left[\left(\frac{\sigma_{\rm h}}{r-2R}\right)^{\nu} - \left(1-(r-2R)\frac{\nu}{\sigma_{\rm h}}\right)\right] \qquad (2)$$

for $2R \le r \le 2R+\sigma_{\rm h}$, with $V_{\rm h}(r) = 0$ otherwise. We then choose a shell size $\sigma_{\rm h} = (2^{1/6}-1)2R$ such that the onset of this steep repulsive interaction at particle separations $r = 2R+\sigma_{\rm h}$ coincides with the minimum in the Lennard-Jones potential at $r = 2^{1/6}\sigma_{\rm LJ} = 2^{7/6}R$. See the thin solid line in Fig. 1. The divergence of this additional contribution as $r \to 2R^+$ then prohibits overlaps in which squirmers approach each other to a separation of less than twice their hydrodynamic radius.

For simplicity we set the potential amplitudes equal throughout, $\varepsilon_{\rm LJ} = \varepsilon_{\rm h} \equiv \varepsilon$, and use a value for the exponent $\nu = 2$. The final combined pairwise interaction potential $V = V_{\rm LJ} + V_h$ is shown by the thicker solid line in Fig. 1. Although the additional repulsive shell provided by $V_{\rm h}$ is not needed for the PBP or ABP (recall that we include it simply to avoid occasional hydrodynamic overlaps in the squirmers), we use it for the Brownian models too to ensure a consistent potential in all simulations, thereby allowing a truly direct comparison between all three models.

The presence of this steeply repulsive shell acts to confer an increased effective disk radius $R_{eff} = R+\sigma_{\rm h}/2$ that slightly exceeds the bare disk radius R. Accordingly we define an effective area fraction $\phi = N\pi R_{eff}^2/L^2$ that likewise slightly exceeds the bare one. Whenever we quote an area fraction throughout the rest of the paper, it is this effective quantity ϕ.

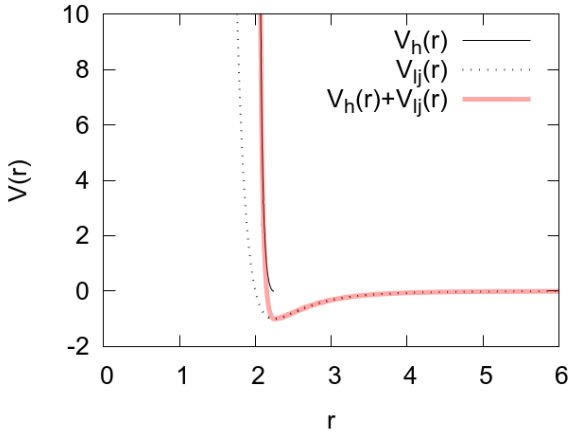

Fig. 1 Modified Lennard-Jones potential in units of ε=1, R=1. Lengthscales $\sigma_{\rm LJ} = 2$ and $\sigma_{\rm h} = 2(2^{1/6}-1)$.

2.2 Dynamics

2.2.1 Passive Brownian particles (PBP).

Before considering active suspensions, which are the primary focus of this work, we will first consider passive Brownian particles (PBP) subject to the same modified Lennard-Jones potential discussed above. We shall do so in order first to establish the equilibrium phase behaviour of a system of particles with this modified

potential, which will then serve as a point of reference for studying the non-equilibrium phase behaviour of active systems subject to the same potential, both without (ABP) and with (HS) hydrodynamic interactions.

Within the model of passive Brownian dynamics, the position $\mathbf{r}_i$ of the ith particle evolves according to

$$\frac{d\mathbf{r}_i}{dt} = -\frac{1}{\gamma}\sum_{j\neq i}\frac{\partial V(|\mathbf{r}_i-\mathbf{r}_j|)}{\partial \mathbf{r}_i} + \sqrt{2D}\Xi_i, \tag{3}$$

with the effect of a solvent coarse-grained in terms of an effective drag of coefficient γ, and with a thermal noise characterised by a diffusion coefficient D. The Gaussian random variable Ξ has

$$\begin{aligned} <\Xi_{i,\alpha}(t)> &= 0, \\ <\Xi(t)_{i,\alpha}\Xi_{j,\beta}(t')> &= \delta_{ij}\delta_{\alpha\beta}\delta(t-t'), \end{aligned} \tag{4}$$

where Latin and Greek symbols denote particle number and Cartesian coordinate respectively. The drag is related to the diffusion constant by the Einstein relation $D = k_{\mathrm{B}}T/\gamma$, where T is the thermodynamic temperature and k_{B} is Boltzmann's constant. The particles also suffer stochastic rotation following Eqn. 6 below, with $D_{\mathrm{r}} = 3D/4R^2$. However this is irrelevant, because the translational dynamics is independent of particle orientation or rotation for these passive particles.

2.2.2 Active Brownian particles (ABP).

Within the model of active Brownian particles, the translational velocity of the ith particle is given by

$$\frac{d\mathbf{r}_i}{dt} = -\frac{1}{\gamma}\sum_{j\neq i}\frac{\partial V(|\mathbf{r}_i-\mathbf{r}_j|)}{\partial \mathbf{r}_i} + v_a\mathbf{e}_i. \tag{5}$$

Besides the effect of the conservative force stemming from the modified Lennard-Jones potential, each particle also moves with a self-propelling velocity $v_a\mathbf{e}_i$. The speed v_a is an imposed constant of the problem. The unit vector $\mathbf{e}_i = (\cos\alpha_i, \sin\alpha_i)$ prescribes the instantaneous preferred direction of self-propulsion, and obeys stochastic angular dynamics governed by a rotational diffusion constant D_{r}, such that

$$\frac{d\alpha_i}{dt} = \sqrt{2D_{\mathrm{r}}}\Xi_i(t). \tag{6}$$

The Gaussian random variable Ξ_i obeys

$$\begin{aligned} <\Xi_i(t)> &= 0, \\ <\Xi_i(t)\Xi_j(t')> &= \delta_{ij}\delta(t-t'). \end{aligned} \tag{7}$$

Note that in an equilibrium system the rotational diffusion coefficient D_{r} would have to relate to the corresponding translational diffusion coefficient D as $D_{\mathrm{r}} = 3D/4R^2$. However the active Brownian particles of interest here do not need to follow any such relation. Indeed, the stochastic angular dynamics prescribed above is not intended to be of true thermal original, but rather as a continuous-time statistical model of (for example) tumbling events in a system of run-and-tumble bacteria, or of particle reorientations occurring via hydrodynamic scattering off other particles. The equivalent rotational diffusion coefficient that characterises these active phenomena is expected be much larger in magnitude than the true thermal one. In order to focus on the effects of activity, therefore, we have removed the thermal noise from the translational equation altogether, setting the translational diffusion coefficient $D = 0$ upfront[24,25]. Indeed we suggest that use of the terminology "Brownian" for ABPs is perhaps better avoided altogether, though we keep it for consistency with the earlier literature.

2.2.3 Hydrodynamic squirmers (HS).

The model of hydrodynamic squirmers is based on a minimal description of microbial propulsion intended to mimic locomotion through a fluid by the beating of many cilia on the surface of a microbe [49,50,54,55,64]. The particles are assumed to be neutrally buoyant and so force free. Their size and swimming speed are sufficiently small that the Reynolds number is assumed negligible (zero inertia) and their swimming dynamics purely Stokesian. Their size is however large enough that Brownian motion (both rotational and translational) is assumed negligible, corresponding to an infinite Péclet number. Other sources of rotational noise such bacteria tumbling are also neglected, and we return to justify this assumption carefully below.

Consider then a monodisperse suspension of N inertialess disk-like swimmers, each of radius R, and each propelling itself through an incompressible Newtonian fluid in the $x-y$ plane by means of an active "squirming" motion modeled by a prescribed tangential velocity

$$S(\theta-\alpha_i) = B_1\sin(\theta-\alpha_i) + \frac{1}{2}B_2\sin 2(\theta-\alpha_i) \tag{8}$$

round the disk edge, at a distance R from the disk's centre. For simplicity this tangential velocity is taken to be time-independent, representing an average over many beating cycles. We denote by $\beta = B_2/B_1$ the ratio of the second and first modes. The sign of β then distinguishes between "pushers" and "pullers", with positive β corresponding to pullers and negative β to pushers. The amplitude of β prescribes the degree of polarity, with $|\beta| \ll 1$ giving strongly polar swimmers and $|\beta| \gg 1$ apolar "shakers".

A single disk undisturbed by any others in an infinite box then has a swim speed $v_0 = B_1/2$[54], with an instantaneous preferred swim direction $\hat{\mathbf{e}}_i = (\cos\alpha_i, \sin\alpha_i)$. In a suspension of many disks the actual swim speeds and directions evolve over time due to hydrodynamic interactions mediated by the Newtonian fluid through which the particles move, as we now describe.

The velocity and pressure fields $\mathbf{v}(\mathbf{r},t)$ and $p(\mathbf{r},t)$ in the fluid outside the disks obey the condition of mass balance for incompressible flow

$$0 = \nabla\cdot\mathbf{v}(\mathbf{r},t), \tag{9}$$

and the condition of force balance in the inertialess limit

$$0 = \eta\nabla^2\mathbf{v}(\mathbf{r},t) - \nabla p(\mathbf{r},t) + \mathbf{f}. \tag{10}$$

Here η is the fluid viscosity and $\mathbf{r} = (x,y)$ is a position vector in the $x-y$ plane. (For convenience the interior of the discs is also taken to contain Newtonian fluid obeying Eqns. 9 and 10. We then

simply discard this part of the mathematical solution, because we are only interested in the behaviour of the fluid outside the disks.)

We recognise Eqn. 10 as the Stokes equation subject to additional source terms $\mathbf{f}$. These represent forces round the edge of each disk:

$$\mathbf{f}(\mathbf{r},t) = \sum_i \mathbf{f}_i(\theta_i)\delta(r_i - R), \tag{11}$$

in which we are summing here over the separate polar coordinate systems (r_i, θ_i) of the disks, such that for the ith disk

$$\mathbf{r} = \mathbf{R}_i(t) + r_i\cos(\theta_i)\hat{\mathbf{x}} + r_i\sin(\theta_i)\hat{\mathbf{y}}, \tag{12}$$

where $\mathbf{R}_i(t)$ is the position of the disk's centre.

These forces are included so as to ensure that the ith disk has at any instant a velocity round its edge

$$\mathbf{v}_i = \mathbf{V}_i - R\Omega_i\hat{\theta}_i + S(\theta - \alpha_i)\hat{\theta}_i, \tag{13}$$

comprising solid body translation and rotation, plus the tangential squirming motion prescribed by the slip velocity function in Eqn. 8 above.

At any timestep $t \to t + Dt$ in the simulation, given a current set of particle positions $\mathbf{R}_i$ and preferred swim directions α_i, known quantities are the lowest two modes of the force (which are constrained to ensure zero total force and torque for each disc, consistent with these particles being swimmers driven by their own internal dynamics and not subject to externally imposed force monopoles or torques), as well as all higher modes of the velocity (as prescribed by the tangential swimming function S). Unknowns to be calculated are the lowest two modes of the velocity, giving the solid body translational velocity $\mathbf{V}_i$ and rotational speed Ω_i. (Also calculated as part of this process are all higher modes of the force, but we do not report these). The particle positions and swim directions are then updated according to $\mathbf{R}_i \to \mathbf{R}_i + Dt\mathbf{V}_i$ and $\alpha_i \to \alpha_i + Dt\Omega_i$.

In this way we exactly (once the numerical mode numbers have been converged upon) solve for the Stokes solution in the fluid outside all the disks, subject to the boundary conditions of the prescribed tangential velocities on the disk edges. Out of this calculation emerge all effects of hydrodynamic interaction, including long range power law propagators, short ranged lubrication effects, and the physics on all lengthscales in between.

For active particles, the Péclet number Pe is defined as the time taken for a particle thermally to diffuse a distance equal to its own radius, divided by the time taken for it to swim the same distance. Here we have assumed this to be infinite, as in Refs.[21,24,27], suppressing Brownian motion entirely and considering only the deterministic hydrodynamics defined above. This is the relevant limit physically for many active suspensions of, *e.g.,* swimming bacteria. We do, however, return to comment further on Péclet number below.

With less justification a priori, we also ignore any intrinsic tumbling dynamics of the particles, such that within our model angular reorientation occurs only via hydrodynamic interactions as the particles scatter off each other. However, as we will explain further in the results section below, we expect this neglect of tumbling to be unimportant, because at the high volume fractions of interest here we find that the relevant physics comes from the high reorientation rate set by these scattering events, which would only be increased still further by the explicit inclusion of tumbling events.

In the literature both spherical (3D)[50] and cylindrical (2D)[54] versions of this squirmer model have been studied. For computational efficiency we use the 2D model[54], which in fluid mechanical terms effectively corresponds to infinitely long (in the z direction) squirming cylinders propelling themselves in the plane $x-y$ that is orthogonal to their length. While this geometry is of course to some extent artificial (as in all studies of reduced dimensionality), it is important to realise that concerns about the famous Stokes catastrophe of 2D hydrodynamics are not relevant here. That catastrophe applies specifically to the case of a particle subject to a force monopole, whereas the swimmers of interest here are force free overall, experiencing only higher order force multipoles. Indeed in a previous publication[28] we carefully compared this 2D case of infinite cylinders to a more realistic 3D scenario of squirming disks of finite thickness (*i.e.* highly flattened cylinders) in a highly viscous film of the same thickness, surrounded by a fluid of much lower viscosity. Reassuringly we found no qualitative difference between these cases, giving confidence that our 2D calculations provide a good representation of the physics of suspensions of squirmers with hydrodynamics.

3 Units and parameter values

Table 1 summarizes the parameters of the problem, defining the simulation geometry, particle size, modified Lennard-Jones potential and the dynamics of the three models. Throughout the paper we work in units of length in which the particle radius $R = 1$, of modulus in which the potential energy $\varepsilon = 1$, and of time in which the drag coefficient $\gamma = 1$ (for Brownian particles) or the Newtonian viscosity $\eta = 1$ (for hydrodynamic squirmers).

Because of the heavy computational cost of the hydrodynamic simulations (recall that we solve the Stokes equation fully in the plane, recovering out of this calculation both far field power law propagators, near field lubrication effects, and the physics on all lengthscales between these), the number of squirmers that we can feasibly simulate is strongly constrained. Here we choose $N = 242$. The more obvious choice of $N = 256$ carries a greater risk of lattice defects at area fractions approaching close packing. We have also checked that the phenomena we report are robust against doubling N. For the Brownian dynamics (both passive and active) many more particles would be possible because of the much lower computational demand of those simulations: up to $N = 10^5$ or $N = 10^6$ Brownian particles can be simulated in run times comparable to those for $N = 242$ hydrodynamic squirmers. However we restrict ourselves to $N = 242$ for the PBP and ABP as well, in order to ensure a direct comparison between all the models. We return at the start of Sec. 6 below to comment carefully on the extent to which one might expect to capture a system's phase behaviour with such a small number of particles.

The lengthscales σ_{LJ} and σ_{h} associated with the potential are set as discussed in Sec. 2.1 above and summarised again in table 1.

An important parameter that then remains to be varied in the

Quantity	Symbol	Dimensions	Dimensionless form	Value	PBP	ABP	HS
Particle radius	R	L	1	length unit	✓	✓	✓
Potential energy	ε	GL^3	1	modulus unit	✓	✓	✓
Drag coefficient	γ	GTL	1	time unit for PBP/ABP	✓	✓	×
Solvent viscosity	η	GT	1	time unit for HS	×	×	✓
Number of particles	N	1	N	242	✓	✓	✓
Potential shell size	$\sigma_{\rm h}$	L	$\tilde{\sigma}_{\rm h}=\frac{\sigma_{\rm h}}{R}$	$2(2^{1/6}-1)$	✓	✓	✓
Lennard-Jones length	$\sigma_{\rm LJ}$	L	$\tilde{\sigma}_{\rm LJ}=\frac{\sigma_{\rm LJ}}{R}$	2	✓	✓	✓
Effective area fraction	ϕ	1	ϕ	to be varied (all models)	✓	✓	✓
Thermal diffusion coefficient	D	L^2T^{-1}	$\tilde{D}=\frac{D\gamma}{\varepsilon}$	to be varied (PBP)	✓	×	×
Rotational diffusion coefficient	$D_{\rm r}$	T^{-1}	$\zeta^{-1}=\frac{D_{\rm r}R}{v_{\rm a}}$	to be varied (ABP)	–	✓	×
Active swim speed	v_a	LT^{-1}	$\tilde{v}_{\rm a}$	to be varied (ABP + HS)	×	$\frac{v_a\gamma R}{\varepsilon}$	$\frac{B_1\eta R^2}{2\varepsilon}$
Active polarity	β	1	β	to be varied (HS)	×	×	✓

Table 1 Parameters for passive Brownian particles (PBP), active Brownian particles (ABP) and hydrodynamic squirmers (HS) with modified Lennard-Jones interactions. Note that PBP are rotationally symmetric so rotational diffusion is unimportant. We work in dimensions space GLT of modulus G, length L and time T, rather than the more usual MLT with M being mass.

simulations for all three models is the area fraction ϕ. Because of the strong repulsive force characterized by the small shell length $\sigma_{\rm h}$, it is reasonable to work with the effective area fraction defined above rather than the bare area fraction $\phi_r = N\pi R^2/L^2$. The real area fraction in practice of course depend on the ratio between the temperature (or active velocity) and the potential energy ε. However the steepness of the repulsive shell's potential renders this effect small in practice. Therefore in what follows, unless stated explicitly otherwise, we report the effective area fraction. Our simulation method allows us to study high area fractions even for hydrodynamic squirmers, and accordingly we shall explore right across the range from dilute towards close packed.

Besides the area fraction, the other important parameters that remain to be varied are as summarised follows. For the passive Brownian particles we have the adimensionalised translational diffusional coefficient $\tilde{D}$, which is also equivalent to the adimensionalised thermodynamic temperature. For the active Brownian particles we have the adimensionalised active swim speed $\tilde{v}_{\rm a}$ and adimensionalised rotational diffusion coefficient ζ^{-1}. Finally for the hydrodynamic squirmers we have the adimensionalised active swim speed $\tilde{v}_{\rm a}$ and the stresslet parameter β. We shall return to discuss in more detail the physical meaning of each of these adimensional quantities in each of the individual subsections concerning PBP, ABP and HS below.

4 Initial conditions

In each run the system is initialised by placing the particles at random positions and with orientations likewise chosen at random from a top hat distribution between 0 and 2π. Obviously some particles will inevitably overlap after this procedure. Overlaps are then removed by evolving the system with zero-temperature dynamics in a landscape of mutual particle repulsion.

We anticipate (but have not checked explicitly) that in any regions of the phase diagram where our simulations attain steady state, that state would be independent of the initial conditions. However, as we shall discuss below, at low temperatures and area fractions we typically find a regime of coarsening dynamics in which the average cluster size slowly increases with time. Due to the very slow dynamics we have not been able to attain steady state in any feasible run time in that regime, and these states must inevitably depend on the initial conditions.

5 Measured quantities

In this section we describe the various quantities that we measure in our simulations in order to analyse clustering and phase behaviour across the different models.

5.1 Snapshots

In each case we first make a simple visual observation of snapshots of the system's configuration, on a grid of values of the area fraction and adimensionalised temperature (or activity parameter). Unless otherwise stated the snapshots shown are in steady state, verified by confirming that the time signals of the mean cluster size, mean particle velocity, *etc.* have attained their final values (which are of course subject to fluctuations). Where stated, in some cases of extremely slow coarsening at low temperature, the snapshots shown are for the longest times that are feasibly accessible numerically.

5.2 Cluster analysis

We statistically analyse the degree of clustering in the system using a single-link algorithm, the details of which are described in Refs.[56,57]. Any two particles are taken to be in the same cluster if their separation r is smaller than a cutoff value $r = r_c$. Indeed it is worth reiterating that any two groups of particles are taken to belong to the same cluster even if only a *single* pair of particles, one in each group, satisfies this cutoff condition. We choose a value for the cutoff separation $r_c = 2.4R$, which just exceeds the value of the particle separation at the minimum in the potential at $r = 2^{1/6}2R \approx 2.24R$. We have checked the robustness of our results to reasonable variations in the value of this cutoff. Common practice in the literature[46,48] is to use a cutoff smaller than the first minimum of the radial distribution function, and we have followed that convention here.

Using this algorithm we measure the cluster size distribution $p(n,t)$ at any instant of time t, and the first moment $\bar{n}(t)$ of this distribution, which gives the mean number of particles per

cluster. We usually report this quantity once the system has reached a statistically steady state after many time units, and time-averaged over a time interval Δt to ensure good statistics. Typically $\Delta t = 310^3R^2/3D$ for PBP, $\Delta t = 3\times10^3R/3v_a$ for ABP and $\Delta t = 10^3R/3v_a$ for HS. In a few, explicitly stated, cases of extremely slow coarsening at low temperature the cluster size is reported at the longest times that are feasibly accessible numerically, again time averaged over Δt.

The instantaneous (non time averaged) behaviour of $\bar{n}(t)$ as function of time t (after initialising the system in a disordered configuration at time $t=0$ as described in Sec. 4) will also be used to to characterise the dynamical coarsening of clusters in the system.

5.3 Particle number fluctuations

In order to gain insight into fluctuations in the local area fraction of particles, we divide the simulation box into a grid of $G\times G$ cells each of dimension $L_G = L/G$, with a typical value of $G=5$. We then define the instantaneous local particle number in each cell i of the grid as $N_i(t)$ and write this as the sum of the average value plus a fluctuation away from this:

$$N_i(t) = \frac{N}{G^2} + \delta N_i(t), \tag{14}$$

and measure the number fluctuations as

$$\delta_N = \langle\sqrt{\langle\delta N_i(t)^2\rangle_i}\rangle_t, \tag{15}$$

which we typically report scaled by $\sqrt{\bar{N}}$, with $\bar{N} = \langle N_i(t)\rangle_i = N/G^2$. Here $\langle\cdot\rangle_t$ represents an average over time, and $\langle\cdot\rangle_i$ an average over particles.

Alternatively we can think in terms of the local area fraction $\phi_i(t) = N_i(t)\pi R^2/L_G^2 = N_i(t)\phi G^2/N$, which for a given grid division G and total number of particles N is related to the local number of particles $N_i(t)$ by a constant factor that depends only on the global average area fraction ϕ. The local area fraction fluctuations are then defined as

$$\delta_\phi = \langle\sqrt{\langle\delta\phi_i(t)^2\rangle_i}\rangle_t. \tag{16}$$

To connect these two measures we note simply that $\delta_\phi/\phi = G^2\delta_N/N$. In what follows below we sometimes find it convenient to report δ_N, which more effectively shows fluctuations at low ϕ, and sometimes δ_ϕ, when focusing on higher ϕ. (The values of $G=5$ and $N=242$ are the same in all our simulations.)

5.4 Hexatic order parameter

While the cluster size distribution and particle number fluctuation measures described so far are effective at discerning the degree of aggregation, they are poorly suited to differentiating between liquid and solid phases. We therefore define a hexatic order parameter Ψ_6 to do this.

We start by defining an instantaneous particle-based local hexatic order, for a given particle j at any time t:

$$\Psi_{6j}(t) = \frac{1}{\hat{n}_j}\sum_{k=1}^{\hat{n}_j} e^{i6\theta_{jk}(t)}. \tag{17}$$

Here $\hat{n}_j$ is the number of neighbours of particle j, defined as those particles inside a threshold separation $r < r_c = 2.4R$, while $\theta_{jk}(t)$ is the angle of the bond between particles j and k.

From this instantaneous particle-based measure of local hexatic order one can then define various different measures of global hexatic order. See[58] for two definitions. Here we focus specifically on the one that averages Ψ_{6j} in time $\langle\cdot\rangle_t$ first for each particle, and then averages the modulus of this quantity over all particles $\langle\cdot\rangle_j$ to give

$$\Psi_6 \quad = \quad \langle|\langle\Psi_{6j}(t)\rangle_t|\rangle_j. \tag{18}$$

For a single perfectly hexatically ordered crystal we expect $\Psi_6 = 1$, while for a totally disordered phase $\Psi_6 = 0$.

6 Results

We now present the results of our simulations. Even though the equilibrium phase behaviour of passive Lennard-Jones (LJ) particles has been mapped out previously, both in 2D[51] and 3D[52], we shall nonetheless start in Sec. 6.1 by studying the equilibrium phase behaviour with our modified LJ potential, which includes the repulsive shell added to avoid particle overlaps for the squirmers. We do so in order to allow in later sections 6.2 and 6.3 a truly direct comparison of the non-equilibrium phase behaviour of active particles - both without and with hydrodynamics - with the equilibrium phase behaviour of their passive counterpart experiencing exactly the same interaction potential, including this repulsive shell. (We do not perform simulations of passive particles with hydrodynamics, because the phase behaviour of equilibrium systems depends only on the static interaction potential and not the dynamics.)

Because the number of particles that we can access for the hydrodynamic squirmers is heavily limited by computational cost (we use $N=242$), it is furthermore important to establish in this more familiar equilibrium context to what extent phase behaviour can feasibly be discerned with such a small system size. Although this number of particles is of course very small for systems without hydrodynamics, by the standards of today's computational capabilities, it is worth noting that the early papers to map out the phase behaviour of Lennard-Jones and hard sphere systems did so using typically $200-1000$ particles[51–53], even in 3D. Indeed these early works established that surprisingly small numbers of particles are needed to map the overall features of the phase diagram correctly. Accordingly we claim that our $N=242$ simulations can capture the main features of phase behaviour. However we do not claim full quantitative statistical analysis of two phase regions, or even less of critical points, to be a realistic goal in this work.

6.1 Passive Brownian particles

As an aid to the reader's memory we start by sketching in Fig. 2 the main features of the equilibrium phase diagram of particles experiencing unmodified LJ interactions, in the plane of adimensionalisation diffusion coefficient $\tilde{D}$ versus the area (or volume) fraction ϕ. Recall that $\tilde{D} = D\gamma/\varepsilon = k_BT/\varepsilon$ measures the thermal energy of the system relative to the characteristic energy of the modified Lennard-Jones potential. As noted above this phase dia-

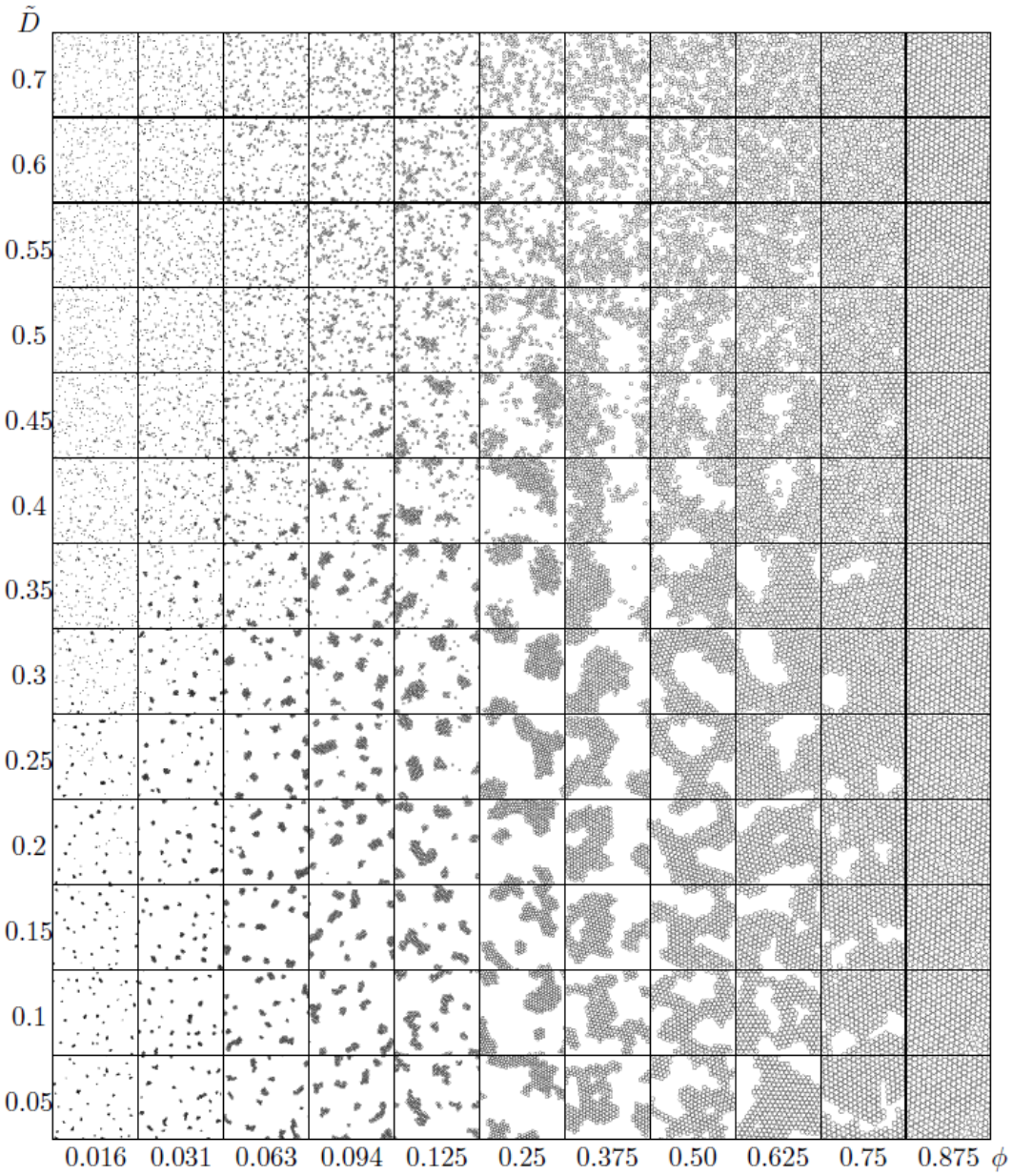

Fig. 3 Passive Brownian particles. Snapshots of the system's configuration on a grid of values of the scaled thermal diffusion coefficient $\tilde{D}$ and area fraction ϕ. Each snapshot is taken at a long time $t = 10^3 R^2/D$ after the system was initialised at $t = 0$ in a random state as described in Sec. 4. Note that the scale is nonlinear at the largest $\tilde{D}$ and at low ϕ.

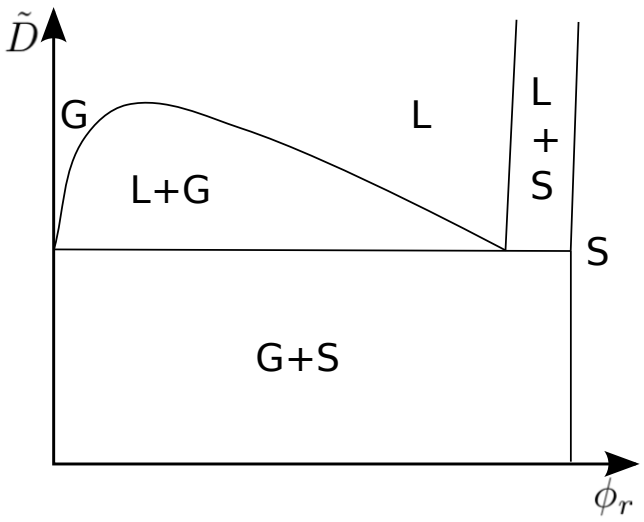

Fig. 2 Sketch of the main qualitative features of the equilibrium phase diagram of disks with a Lennard-Jones interaction potential $V_{\rm LJ}$ [52,59]. S=solid, L=liquid, G=gas.

gram has been comprehensively mapped out previously [51,52]. Indicated are the single phase regions of gas (G), liquid (L) and solid (S), and the phase coexistence regions G-L, G-S, L-S. We emphasize that Fig. 2 is a rough qualitative sketch only, with no attempt at quantitative accuracy.

Turning now to our modified Lennard-Jones potential, we show in Fig. 3 snapshots of the system's configuration on a grid of values $\tilde{D}$ and area fraction ϕ. All snapshots shown are for the longest time that is feasibly accessible computationally. At low temperatures, $\tilde{D} \lesssim 0.4$, aggregated domains are evident across the full range of area fractions. These coarsen very slowly as a function of time, and at the lowest area fractions and temperatures (typically in the rectangle of phase space with $\phi < 0.125$ and $\tilde{D} < 0.4$) this process cannot be evolved fully to steady state within a feasible run time. (For example, an order of magnitude estimate suggests that for the simulation at $\phi = 0.0125$ and $\tilde{D} = 0.05$ to have fully coarsened, a run time of about 6 months involving $O(10^9)$ timesteps would have been needed.) The snapshots in this region are therefore not in true steady state, though we are confident that the qualitative features will not change even for longer run times, which would simply result in slightly larger clusters. At higher temperature we have checked that the system is in steady state.

Simple visual inspection of these snapshots suggests an overall structure to the phase diagram that indeed captures the main features of the sketch in Fig. 2. In particular, a G-S coexistence region is visually apparent for $\tilde{D}$ less then about 0.35. Above this, a G-L coexistence region extends up towards what resembles a critical point somewhere in the region of $\phi = 0.4$ and $\tilde{D} = 0.55$. However we do not focus on this critical point in detail because we do not have sufficient particles in our simulation to characterise it properly. For high area fractions, roughly $\phi > 0.7$, solid-like ordering is evident even at high temperatures. This area fraction for the onset of solid ordering is lower than that expected for particles with conventional LJ interactions, but is consistent with the fact

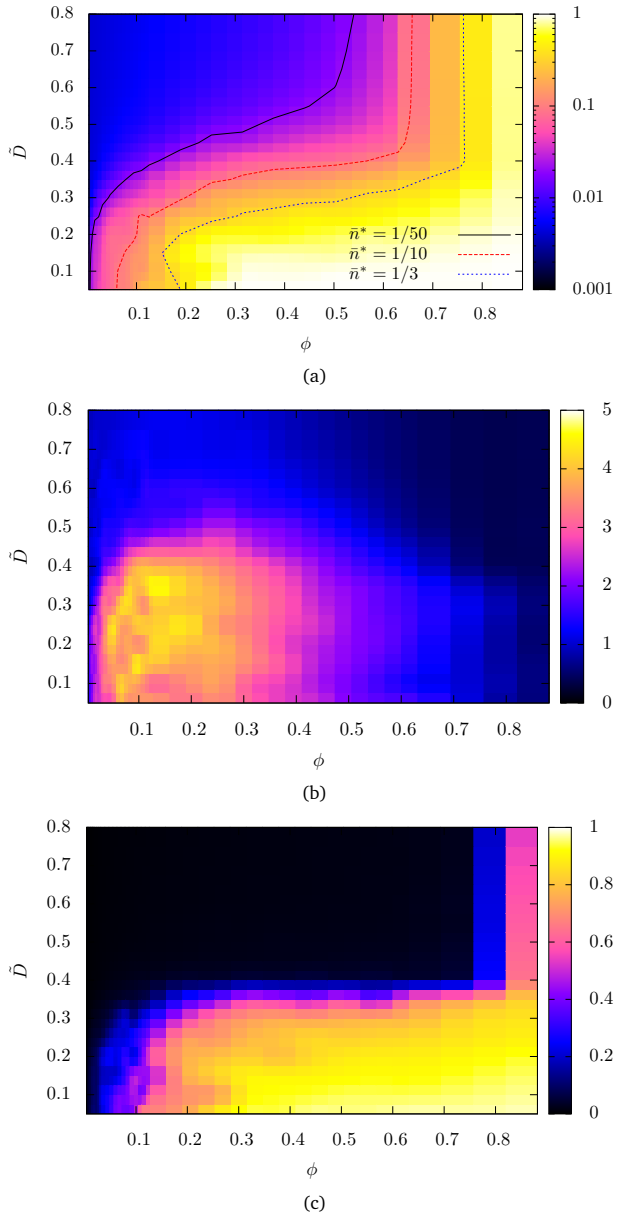

Fig. 4 Phase diagram of passive Brownian particles mapped using (a) normalised mean number of particles per cluster $\bar{n^*} = \bar{n}/N$, (b) particle number fluctuations $\delta_N/\sqrt{\bar{N}}$ for $G = 5$ and c) hexatic order parameter Ψ_6.

that our modified LJ potential includes an effectively hard shell repulsion at $r = 2R$.

To try map the phase diagram more quantitatively, we show in Fig. 4 colour maps of the statistical measures introduced in Sec. 5 above. Subfigure (a) shows the mean number of particles per cluster, normalized by the total number of particles in the system: $\bar{n}^* \equiv \bar{n}/N$. Note that a system-spanning homogeneous phase with all particles in same cluster would have $\bar{n}^* = 1$, while a gas phase with no clusters would have $\bar{n}^* = 1/N$, which is small for large N. With this in mind we have also marked on the colourmap isolines of $\bar{n}^* = 1/50, 1/10, 1/3$, which correspond to $\bar{n} = 4.84, 24.2, 80.7$ for our $N = 242$. We suggest that the region in between the first two of these corresponds to one of clusters of a finite size $\bar{n} > 1$,

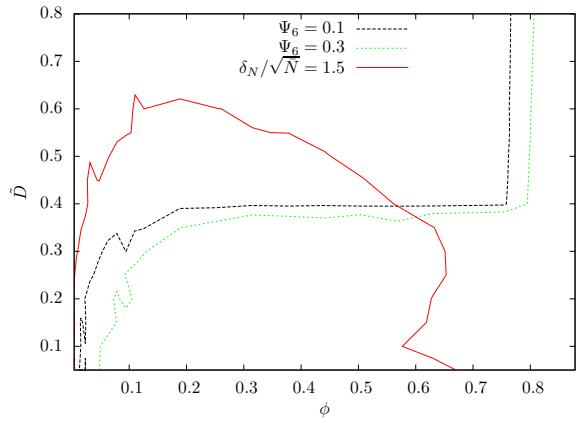

Fig. 5 Representative isolines of particle number fluctuations $\delta_N/\sqrt{N} = 1.5$ and $\Psi_6 = 0.1, 0.3$. Regions broadly consistent with the sketch of Fig.2 are evident.

but which do not yet span the full system size $\bar{n}^* = 1$. Comparison with simulations of larger N would however be needed to substantiate this claim properly. Note that, as above for the snapshots, in the region roughly given by $\phi < 0.25$ and $\tilde{D} < 0.4$ the clusters are still coarsening so that waiting for an even longer run-time would result in a larger $\bar{n}$.

Subfigure (b) shows the particle number fluctuations $\delta_N/\sqrt{N}$, measured by dividing the simulation box into a grid of $G \times G = 5 \times 5$ subunits. Clearly apparent is a region with strongly enhanced number fluctuations, which we suggest can be interpreted as a region of phase coexistence. However this measure provides no means of distinguishing between a phase coexistence that involves only disordered phases, $G-L$, from one involving the ordered solid phase, $G-S$ or $L-S$. In any case it is strongly suppressed at high volume fractions $\phi > 0.7$ and so fails altogether as an indicator of phase separation in this regime.

To try identify these solid regimes, we show in subfigure (c) a colour map of the hexatic order parameter. The bright region for $\phi > 0.75$ clearly indicates the presence of crystalline ordering. We further suggest the region $\tilde{D} < 0.35$ to be one of $G-S$ coexistence (or fully solid at high ϕ, but this cannot be discerned separately), consistent with visual inspection of the snapshots in Fig. 3. (For small area fractions the solid component is too weak to show in this representation. As noted above, however, in this part of the phase diagram coarsening is so slow that this system does not attain a true steady state within the run time.) We also suggest that for $\tilde{D} > 0.35$ the region $0.75 < \phi < 0.8$ is one of $L-S$ coexistence, and that of $\phi > 0.8$ a homogeneous S phase. We emphasize however that these boundaries are suggestive only, and that simulations with far more particles would be needed to provide quantitatively conclusive evidence.

Finally we assemble in Fig. 5 a representative isoline of the particle number fluctuations $\delta_N/\sqrt{N} = 1.5$ together with two representative isolines of the hexatic order parameter $\Psi_6 = 0.1, 0.3$, revealing a phase diagram that indeed qualitatively resembles the sketch in Fig. 2.

Although our main aim in this section has been to report equilibrium phase behaviour, we return finally to reiterate that in the rectangle of phase space with $\phi < 0.25$ and $\tilde{D} < 0.4$ the system doesn't equilibrate in any feasible run time but rather shows a slow coarsening behaviour in which the typical cluster size increases as a power law $\bar{n} \sim t^{\beta}$. A value for the exponent $\beta = 2/3$ provides an excellent fit to the data (not shown), consistent with the expectation[60] of a linear domain size growing as $L \sim t^{1/3}$. Although we have been careful only to extract data for the coarsening exponent in regimes where the typical cluster size is less than the system size, a more detailed study of the model's coarsening dynamics, for which finite size effects should be investigated carefully, is out of the scope of this paper.

6.2 Active Brownian Particles

In the previous subsection we mapped out the equilibrium phase behaviour of passive Brownian particles (PBPs) in the plane of area fraction ϕ and adimensional diffusion coefficient $\tilde{D} = D\gamma/\varepsilon = k_B T/\varepsilon$, which measures the system's thermal energy compared with the characteristic energy ε of the modified Lennard-Jones potential. As discussed, we recovered the main features of phase behaviour expected from previous studies of Lennard-Jones particles, with some differences consistent with our use of an additional steep repulsive contribution V_h.

We turn now to active Brownian particles (ABPs). Although the phase behaviour of ABPs with unmodified Lennard-Jones interactions has been studied previously[47], we will map it out here for our modified Lennard-Jones potential using the same small number of particles $N = 242$ as will be feasible to explore computationally for the hydrodynamic squirmers in Sec. 6.3 below. This will then enable a truly direct comparison between ABPs, which lack hydrodynamic interactions, and squirmers, which have them.

As discussed above, the ABPs move via ballistic swimming at speed $\tilde{v}_a$ combined with stochastic reorientational dynamics with angular diffusion coefficient D_r. The latter is intended as a continuous time model of (for example) discrete tumbling events, in some species of bacteria, or reorientations due to hydrodynamic scattering off other swimmers. It is not intended to model true thermal angular diffusion, which would be much smaller in comparison. Indeed, as noted above, we consider here the athermal limit in which any thermal contribution to D_r is zero, which is the relevant limit for many swimming microbes.

Despite this lack of true thermal translational diffusion, an obvious question to ask is whether the activity of the ABPs (ballistic swimming combined with stochastic reorientation) plays a role somewhat akin to the thermal diffusive dynamics of the PBPs, such that the non-equilibrium phase behaviour of the ABPs is in some degree analogous to the equilibrium phase behaviour of the PBPs. For example, we might intuitively anticipate phase separation at small v_a due to the attractive effects of the Lennard-Jones potential, with a return to homogeneous behaviour at large v_a where the activity is strong enough to overcome that attraction. In what follows, therefore, we will seek to compare the equilibrium phase behaviour of PBPs in the plane of $(\tilde{D}, \phi)$, as mapped out above, with the non-equilibrium phase behaviour of the ABPs in the plane of (v_a, ϕ), with v_a first suitably adimensionalised.

However, whereas for PBPs the only two relevant parameters

were indeed $\tilde{D}$ and ϕ, for ABPs the rotational diffusion coefficient D_r is also important, alongside v_a and ϕ. The reason for this is as follows. In the case of spherical PBPs rotational diffusion, though surely present physically, is irrelevant: each particle is rotationally symmetric and the translational dynamics is accordingly independent of particle orientation. In contrast, for ABPs the translational dynamics depends strongly on the orientational dynamics, because the instantaneous preferred swimming direction of any particle is (by definition) prescribed by its instantaneous orientation. In view of this we must actually consider the phase behaviour of ABPs in the plane of (v_a, ϕ) for several different values of D_r, with both v_a and D_r first suitably adimensionalised.

To adimensionalise the rotational diffusion coefficient D_r we define a parameter[28]

$$\zeta = \frac{v_a}{D_r R f(\phi)} = \frac{\tau_o}{\tau_c(\phi)}, \tag{19}$$

which is the ratio of the characteristic decorrelation time of the particle's orientation (swim direction)

$$\tau_o = \frac{1}{D_r} \tag{20}$$

with the characteristic time interval between particle collisions

$$\tau_c = \frac{R f(\phi)}{v_a}. \tag{21}$$

Here $f(\phi)$ is an adimensional function that we expect to decrease with increasing ϕ. In the dilute gas limit of small ϕ we would estimate $f = \pi/\phi$ from mean free path arguments, while for more crowded systems with $\phi = O(1)$ we might instead simply assume $f = O(1)$. Because our main focus in this paper concerns moderately to highly crowded systems, $\phi = O(1)$, for simplicity we set $f = 1$ throughout. Accordingly we work simply with

$$\zeta = \frac{v_a}{D_r R}. \tag{22}$$

In the regime $\zeta \ll 1$, particles change their orientation many times during a typical interval between collisions. Therefore the dynamics during an interval $0 < t < \tau_c$ between any two collisions will comprise only a proportionately much shorter regime of ballistic motion at speed v_a for times $0 < t < \tau_o \ll \tau_c$, followed by a longer diffusive regime for times $\tau_o < t < \tau_c$. In this way the "microscopic" (pre-collision) dynamics that feed forward to inform the collisional dynamics are predominantly diffusive, with an effective diffusion coefficient v_a^2/D_r. It might then be reasonable to expect that the phase diagram of the ABPs will mirror that of the PBPs with the scaled diffusion coefficient $\tilde{D} = D\gamma/\varepsilon$ of the passive system replaced its scaled counterpart $v_a^2\gamma/D_r\varepsilon$ for the active one.

In contrast, in the regime $\zeta \gg 1$ the dynamics of the ABPs will be dominated by ballistic swimming over the entire time between collisions, with the slow angular reorientation being relatively unimportant in comparison. In this case it is less clear, upfront, what correspondence might be expected between the phase diagram of the ABPs with its equilibrium counterpart for the PBPs. As elaborated further below, however, we will indeed find some correspondence in the regime of low activity.

This existence of two different regimes of the dimensionless inverse angular diffusion coefficient ζ points to two different possible choices for adimensionalising the swim speed v_a. The first, which we expect to be the natural choice in the regime $\zeta \ll 1$, takes into account both ballistic swimming and angular reorientation by recognising that v_a^2/D_r has the dimensions of a translational diffusion coefficient then writing $\tilde{\tilde{v}}_a = v_a^2\gamma/D_r\varepsilon$, by direct analogy with $\tilde{D} = D\gamma/\varepsilon$ for the PBPs.

The second choice, which we expect to be the natural one in the regime $\zeta \gg 1$, considers only the ballistic component of the swimming dynamics, taking the ratio of v_a with the characteristic speed $\varepsilon/R\gamma$ that a particle would exhibit when subject to a force of magnitude ε/R in a solvent of drag coefficient γ. This gives an adimensionalised swim speed $\tilde{v}_a = v_a R\gamma/\varepsilon$ that ignores the angularly diffusive component of the dynamics as characterised by D_r. It is nonetheless still seen as a possible counterpart of the $\tilde{D}$ of PBPs by writing $\tilde{D} = D\gamma/\varepsilon = (D/R)R\gamma/\varepsilon$, and noting that D/R has dimensions of speed. We note that for $\zeta = 1$, $\tilde{v}_a = \tilde{\tilde{v}}_a$ and the two methods of adimensionalising v_a coincide, as required.

With this preamble in mind, we now present results for the phase behaviour of ABPs in the plane of (v_a, ϕ) for two values of the adimensional inverse diffusion coefficient ζ, one in each regime just described, with the swim speed v_a in each case first adimensionalised in a manner suited to the value of ζ according to the arguments just outlined. Where useful, we will also further present results in the plane of $(\tilde{v}_a, \zeta)$ for different values of ϕ.

We start in Fig. 6 by showing long-time snapshots of the system's configuration on a grid of values of $(\tilde{\tilde{v}}_a, \phi)$ for a low value of the scaled inverse diffusion coefficient $\zeta = 0.2$. Immediately apparent is that this non-equilibrium phase diagram displays striking similarities to its equilibrium counterpart for the PBPs in the plane of $(\tilde{D}, \phi)$: recall Fig. 3. In particular, a G-S coexistence region is seen for values of $\tilde{\tilde{v}}_a$ less then about 0.4. Above this a G-L coexistence region extends up towards what resembles a critical point somewhere in the region of $\phi = 0.4$ and $\tilde{\tilde{v}}_a = 0.7$, which is quite close to that identified above for the PBP. For high area fraction, solid-like ordering is also again evident. For this small value of ζ, then, the main features of the equilibrium phase behaviour of PBPs transcribe to the non-equilibrium ABPs, with the scaled temperature $\tilde{D} = k_B T/\varepsilon$ replaced by the scaled swim speed $\tilde{v}_a$.

Again as for the PBP, in a lower-left rectangle of the plane $(\tilde{\tilde{v}}_a, \phi)$ that roughly corresponds to $\phi < 0.25$ and $\tilde{\tilde{v}}_a < 0.4$, the system doesn't reach steady state in any feasible run-time but instead shows a characteristic power-law coarsening process in which the typical domain size grows in time as $\bar{n} \sim t^{\beta}$. The data are well fit by the exponent $\beta = 2/3$, as in the PBP above (data not shown).

We have established, then, that for small ζ the phase behaviour (and coarsening kinetics) of ABP in the plane of $(\tilde{\tilde{v}}_a, \phi)$ closely resembles that of PBP in the plane of $(\tilde{D}, \phi)$. This correspondence is with hindsight perhaps unsurprising, given that the intercollisional dynamics are mainly diffusive in this regime, as in a passive system.

We now turn to the opposite regime of large ζ, where $\tilde{v}_a$ is the most obvious choice for adimensionalising v_a. Fig. 7 shows long-time snapshots of the system's configuration on a grid of values of $(\tilde{v}_a, \phi)$ for $\zeta = 200.0$. The situation here is clearly more

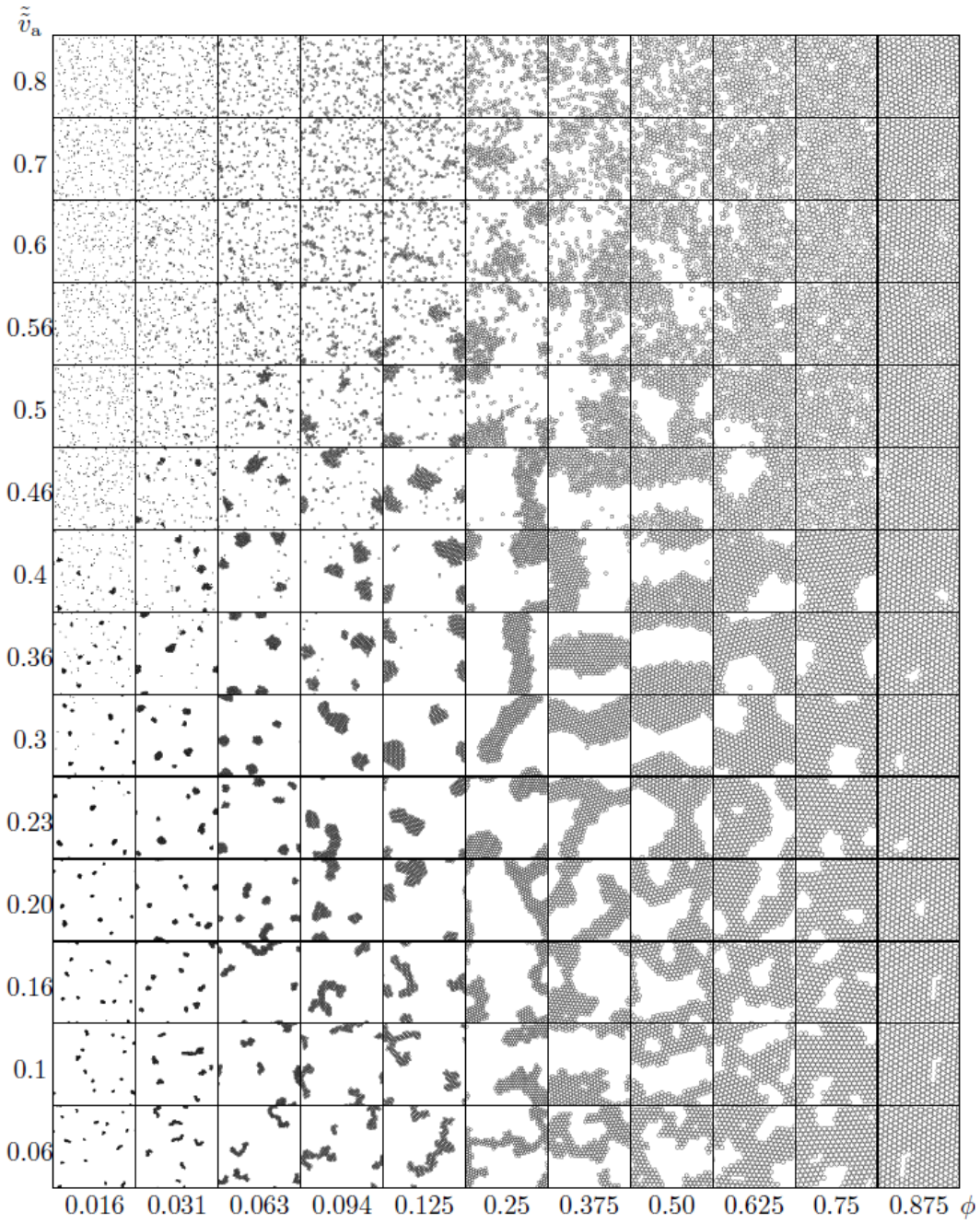

Fig. 6 Active Brownian particles, $\zeta = 0.2$. Snapshots of the system's configuration on a grid of values of the scaled active swim speed v_a and effective area fraction ϕ. Each snapshot is taken at a long time $3 \times 10^3 v_a/R$ after the system was initialised at $t = 0$ in a random state as described in Sec. 4. Note that the scale is nonlinear at the largest $\tilde{v}_a$ and at low ϕ.

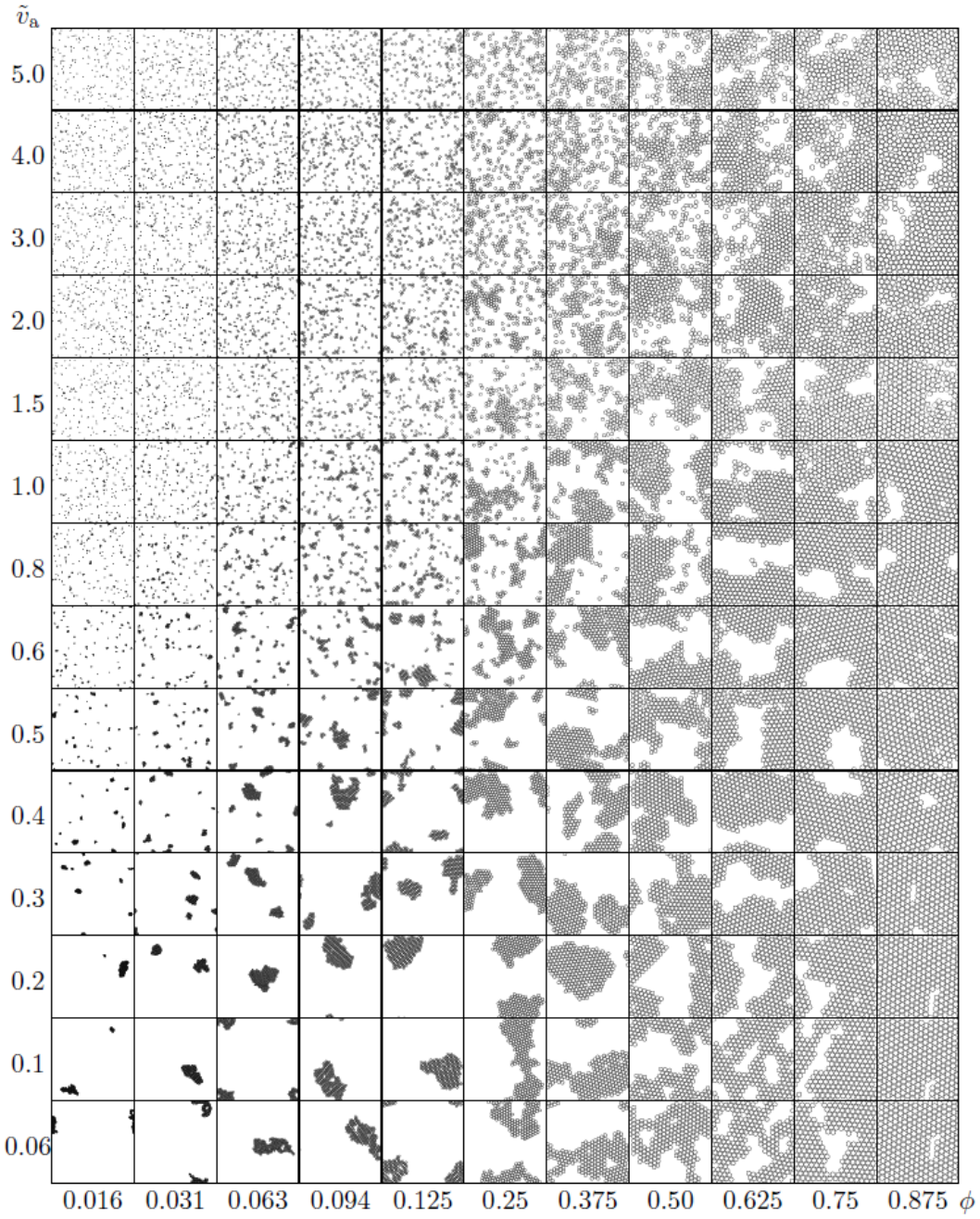

Fig. 7 Active Brownian particles, $\zeta = 200.0$. Snapshots of the system's configuration on a grid of values of the scaled active swim speed v_a and effective area fraction ϕ. Each snapshot is taken at a long time $3 \times 10^3 v_a/R$ after the system was initialised at $t = 0$ in a random state as described in Sec. 4. Note that the scale is nonlinear at the largest $\tilde{v}_\mathrm{a}$ and at low ϕ.

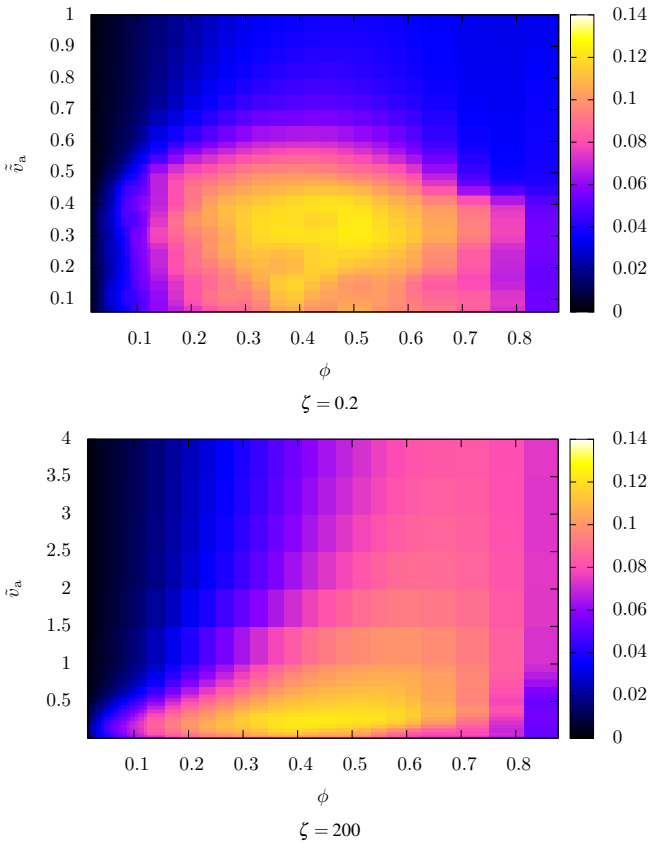

Fig. 8 Active Brownian Particles. Area fraction fluctuations δ_ϕ for a small (upper) and large (lower) value of ζ. Quasi-equilibrium phase separation is seen at low scaled active swim speed v_a for both values of ζ. Strongly non-equilibrium MIPS is seen at high $\tilde{v}_a$ only for large ζ. Number of boxes $G = 5$.

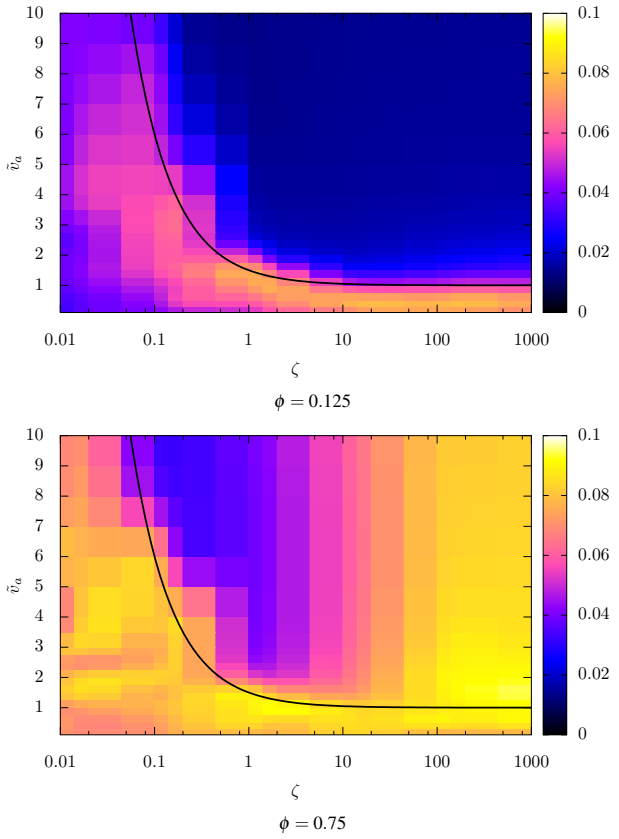

Fig. 9 Active Brownian particles: area fraction fluctuations δ_ϕ in the $\phi - \zeta$ plane. The black line corresponds to the curve $v_a\zeta/(1+\zeta) = 1$. See Eqn. 23 in the main text. Number of boxes $G = 5$.

complicated than for the low value of ζ, with the phase diagram differing more markedly from the equilibrium case. This is to be expected, consistent with the fact that underlying "microscopic" dynamics that feeds forward to inform the collisional dynamics is predominantly ballistic, rather than diffusive as it was in the case either of PBPs or ABPs for small ζ.

Nonetheless, at low swim speeds the phase behaviour does appear rather similar to that of PBPs, and so also of ABPs at small values of ζ. Accordingly we suggest that this again corresponds to a regime of phase separation analogous to that of the equilibrium PBPs, arising due to the dominance of the Lennard-Jones attraction over the active swimming for small v_a. However we repeat that the physics is subtly different here: unlike the equilibrium case the intercollisional dynamics is predominantly ballistic rather than diffusive. In view of this, the fact that we do still see a regime of attraction-dominated quasi-equilibrium phase separation at low $\tilde{v}_a$ is a non-trivial result. On this basis, one might tentatively claim that the ABPs' scaled swim speed has some properties resembling those of a non-equilibrium effective temperature.

At high activity (large $\tilde{v}_a$), however, the phase behaviour for this large value of ζ is markedly different from the equilibrium case. In particular, a second regime of phase separation is evident for values of ϕ exceeding about 0.4. Clearly, this could not have been predicted on the grounds of any direct analogy with the equilibrium phase diagram. How then can it be understood?

For these large values of $\tilde{v}_a$ we expect the strength of swimming to easily overcome any attraction associated with the LJ potential, such that active LJ disks behave effectively as active hard disks in this limit $\tilde{v}_a \to \infty$. With this in mind, we recall previous work for hard disk ABPs that demonstrated a phenomenon known as "motility induced phase separation" (MIPS) [21,22]. This arises via a positive feedback mechanism in which particles (a) accumulate in regions where they move more slowly, then (b) further slow down in regions of accumulation, being impeded by overcrowding from other particles. Note that although part (a) of this mechanism may seem intuitively obvious – think of window shoppers accumulating where they linger near a more interesting display – it is actually a highly non-equilibrium phenomenon: in equilibrium colloids the local density depends only on the static potential and not on any dynamical rules. Informed by this, we interpret this second region of phase separation, seen at high $\tilde{v}_a$ for large ζ, as one of MIPS.

The absence of MIPS at high $\tilde{v}_a$ for small values of ζ, as in Fig. 6, is then further understood [28,61] by realising that part (b) of the feedback mechanism just described contains a mean field assumption that fails for small ζ: in order to experience a slowing down of its run speed, a particle must collide many times during any such run before changing direction. This assumption breaks

down for small values ζ, where particles reorient very quickly on the timescales of interparticle collisions.

This difference between the phase behaviour of ABPs for small and large values of ζ is characterised at a glance by colour maps of the particle number fluctuations in Fig. 8: MIPS is apparent for large ζ (bottom panel) for $\phi \gtrsim 0.5$ and $\tilde{v}_a \gtrsim 1.0$; and absent for small ζ (top panel).

The dependence on ζ is shown more fully in Fig. 9. For the small area fraction $\phi = 0.125$, no MIPS is expected for any value of ζ (recall Fig. 8) and we see only quasi-equilibrium phase separation driven by the Lennard-Jones attractions. As can be seen, this arises for $\tilde{v}_a < O(1)$ at large ζ, consistent with the expectation that $\tilde{v}_a = v_a R\gamma/\varepsilon$ is the relevant scaling variable in this regime. In contrast, for low ζ it arises instead for $\tilde{\tilde{v}}_a < O(1)$, consistent with the expectation that $\tilde{\tilde{v}}_a = v_a^2\gamma/D_r\varepsilon$ is the relevant scaling variable in this regime. Noting that $\tilde{\tilde{v}}_a = \tilde{v}_a\zeta$, we find finally that

$$\frac{\tilde{v}_a\zeta}{1+\zeta} < 1 \tag{23}$$

gives a good fit to the regime of attraction-dominated phase coexistence for all values of ζ, recovering $\tilde{\tilde{v}}_a < 1$ for $\zeta \ll 1$ and $\tilde{v}_a < 1$ for $\zeta \gg 1$.

For the larger area fraction $\phi = 0.75$ in Fig. 9 we find the same picture with regards attraction-dominated phase separation, with the transition again given by Eqn. 23. In addition to this we find a regime of MIPS for large values of $\zeta \gtrsim 10.0$ and $\tilde{v}_a \gtrsim 1.0$. Interestingly, these regimes of equilibrium-like attraction-dominated phase separation and MIPS appear to merge with each other smoothly, with a gradual cross over regime in which both mechanisms contribute. We note that re-entrance between two regimes of phase separation was also observed in simulations of attractive ABPs with the conventional LJ potential in Ref.[47]. However that work considered only the regime of small rotational diffusion coefficient (of thermal origin, and so related to the Brownian diffusion coefficient via a factor $3/R^2$) and therefore necessarily saw a regime with MIPS. The present study goes beyond the findings of[47] in showing MIPS to be suppressed with increasing rotational diffusion. (RB11/15)In Ref.[48], a crossover from equilibrium-like phase behaviour to a non-equilibrium percolating network phase was seen in a system of active Brownian Lennard Jones particles as function of decreasing rotational diffusion coefficient. The percolating network phase in that study might well be the counterpart of the MIPS seen here, though further work would be needed to elucidate further any connection.

6.3 Hydrodynamic squirmers

In the previous section, we explored the phase behaviour of active Brownian particles (ABPs), which combine ballistic swimming with stochastic angular reorientation that is intended to mimic, in continuous-time counterpart, discrete tumbling events in some species of bacteria, or scattering off other particles due to hydrodynamic interactions. Hydrodynamic interactions are not, however, explicitly accounted for in ABPs. In this section we turn to address that shortcoming by studying a suspension of squirmers that do interact hydrodynamically.

We start with a recap of the parameters that characterise squirmers and the appropriate adimensional form of these, as first introduced in Sec. 3 above. Indeed to set these in a proper context, we recall them alongside the (by now) familiar parameters of the PBP and ABPs.

As always we take as fixed the number of particles $N = 242$ and the lengthscales σ_h and σ_{LJ} that set the size of the potential shell relative to the hydrodynamic radius R. For the PBPs the remaining five parameters are then the particle radius R, the potential energy ε, the drag coefficient γ, the area fraction ϕ and the thermal translational diffusion coefficient D. Choosing units of mass, length and time left two remaining dimensionless parameters: $\tilde{D} = D\gamma/\varepsilon = k_BT/\varepsilon$ and ϕ. In Sec. 6.1 we explored the phase behaviour of our modified Lennard-Jones particles in this plane of $(\tilde{D}, \phi)$. For the ABPs the remaining parameters were the particle radius R, the potential energy ε, the drag coefficient γ, the area fraction ϕ, the swim speed v_a and the rotational diffusion coefficient D_r. In dimensionless form these gave three parameters, which we explored numerically in the previous section. Two of these were the area fraction ϕ and the scaled inverse rotational diffusion coefficient $\zeta = v_a/D_rR$, which characterises the time taken for the angular decorrelation of swim direction relative to the typical time interval between particle collisions. The third was the swim speed v_a, for which we argued $\tilde{\tilde{v}}_a = v_a^2\gamma/D_r\varepsilon$ to be an appropriate adimensional form in the regime of small ζ where the inter-collisional dynamics are diffusion dominated, and $\tilde{v}_a = v_aR\gamma/\varepsilon$ at high ζ, where the inter-collisional dynamics are predominantly ballistic. Given that $\tilde{\tilde{v}}_a = \tilde{v}_a\zeta$ these two coincide for values of $\zeta = O(1)$, as desired.

For the hydrodynamic squirmers to which we now turn the relevant parameters are the particle radius R, the potential depth ε, the solvent viscosity η, the area fraction ϕ, the swim speed $v_a = B_1/2$ and the relative stresslet strength $\beta = B_2/B_1$. In dimensionless form we then have the scaled swim speed $\tilde{v}_a = v_a\eta R^2/\varepsilon$, the area fraction ϕ, and the stresslet strength β. We shall show in what follows that the effects of β on phase behaviour are in fact relatively mild. Accordingly we shall focus first, and mainly, on phase behaviour as a function of $\tilde{v}_a$ and ϕ, before returning at the end of the section to comment on the effects of varying β.

Excluding β for the moment, then, we note the number of important parameters $(\tilde{v}_a, \phi)$ for the squirmers to be one fewer than those for the ABPs, ($\tilde{v}_a$, ϕ, ζ) (or $(\tilde{\tilde{v}}_a, \phi, \zeta)$). The reason for this is as follows. Whereas the ABPs have externally imposed reorientation dynamics with a rotational diffusion coefficient D_r, adimensionalised as ζ, the squirmers have no reorientation dynamics imposed upfront. Instead, reorientation events emerge naturally as a result of the hydrodynamic interactions that determine the way in which the squirmers scatter off each other (at low area fraction) or slither round each other (at high area fraction). In consequence we expect an effective ratio $\zeta_{eff} \equiv \tau_o/\tau_c$ of reorientation time to scattering time to emerge naturally from the squirmers' many body hydrodynamics, instead of existing as a free parameter to be imposed at the outset in the simulations.

Having identified the relevant parameters, a natural question is then whether the phase behaviour of the squirmers in the plane of $(\tilde{v}_a = v_a\eta R^2/\varepsilon, \phi)$, with whatever value of ζ_{eff} emerges naturally

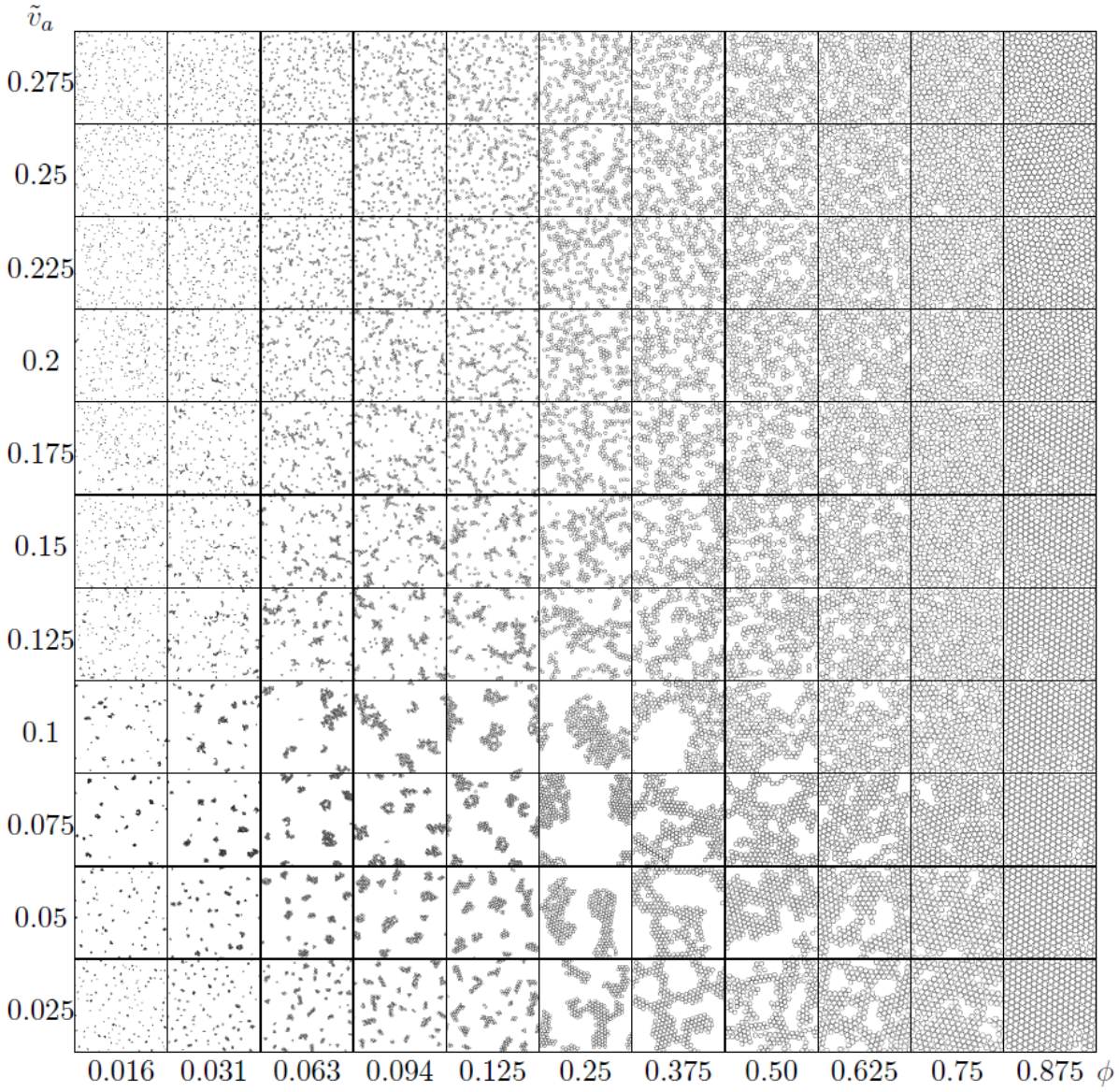

Fig. 10 Hydrodynamic squirmers, $\beta = 0.0$. Snapshots of the system's configuration on a grid of values of the scaled active swim speed $\tilde{v}_a$ and effective area fraction ϕ. Each snapshot is taken at a long time after the system was initialised at $t = 0$ in a random state as described in Sec. 4. In the rectangle $\tilde{v}_a < 0.15$ and $\phi < 0.1$ the system fails to reach steady state in any feasible runtime and instead shows slow domain coarsening. All other snapshots shown are from a system in statistically steady state. Note that the scale is nonlinear at the largest $\tilde{v}_a$ and at low ϕ.

from the hydrodynamic simulations, mimics that of the ABPs in the plane $(\tilde{v}_a = v_a\gamma R/\varepsilon, \phi)$ for a corresponding value of ζ, as imposed for the ABPs. One can of course also further ask whether it further mimics that of PBPs in the plane of $(\tilde{D}, \phi)$.

Clearly, the dimensionless forms for v_a identified above suggest that we might look for a possible correspondence between ABPs and squirmers (after matching the imposed ζ for the ABPs with the emergent ζ_{eff} for the squirmers) upon setting the ABPs' drag coefficient $\gamma = \eta R$, where η is the solvent viscosity for the squirmer simulations. However it should be noted that this expression should also contain a prefactor, which is unknown. The specific case of a sphere dragged by a force monopole through an infinite domain of fluid in 3D gives $\gamma = 6\pi\eta R$. However we are concerned here neither with force monopoles nor with 3D and the prefactor remains unknown, even if we might reasonably expect it to be $O(1)$. With this preamble in mind we now present our results. We start by taking a fixed $\beta = 0.0$ and shall return at the end of the section to comment on the effect of varying β. Fig. 10 shows snapshots of the system's configuration on a grid of values of $(\tilde{v}_a, \phi)$. Each snapshot corresponds to the longest run time that is feasibly accessible computationally. Most represent a statistically steady state, except in a region towards the lower left of the $(\tilde{v}_a, \phi)$ plane, typically for values of $\tilde{v}_a < 0.15$ and $\phi < 0.1$. Here the coarsening dynamics of the aggregated domains, which we shall discuss in more detail below, is sufficiently slow that the system never attains steady state in this regime in any reasonable run time. Despite this we are confident that running for even longer times would not affect the qualitative features of the system's state, apart from giving larger domains.

Some quantitative measures of this phase diagram are shown in Fig. 11. Panel a) gives the mean number of particles per cluster $\bar{n}$, normalised by the total number of particles N to give $\bar{n}^* = \bar{n}/N$. Recall that a single system-spanning condensate would have $\bar{n}^* = 1$, while a gas phase with no clusters would have $\bar{n}^* = 1/N$, which is small for large N. Panel b) shows the particle number fluctuations $\delta_N/\sqrt{\bar{N}}$ measured by dividing the simulation box into $G \times G$ subboxes where $G = 5$. Subpanel c) shows the hexatic order parameter Ψ_6. Recall that regions of high $\bar{n}^*$ and $\delta_N/\sqrt{\bar{N}}$ indicate clustering or phase separation, while regions of high Ψ_6 indicate a high degree of solid-like crystalline ordering.

Comparing these snapshots and colourmaps for the squirmers (Figs. 10 and 11) with their counterparts for the PBPs (Figs. 3 and 4) reveals that the overall phase behaviour of the squirmers loosely mirrors that of the PBPs, with the scaled swim speed $\tilde{v}_a$ playing a role somewhat analogous to that of the scaled diffusion coefficient $\tilde{D}$ of the PBPs. In particular, attraction-dominated phase separation and hexatic ordering appears evident at low $\tilde{v}_a$ (corresponding to low $\tilde{D}$ for the PBPs), giving way to disorder and homogeneity at high $\tilde{v}_a$ (high $\tilde{D}$ for the PBPs) where the particles' activity (thermal jostling for the PBPs) is sufficient to overcome the attractive effects of the potential. Solid-like ordering is also evident in a column of values of $\tilde{v}_a$ for densely crowded systems with $\phi > 0.75$.

However there are also important differences. For example, in the squirmers hexatic ordering (Fig. 11c) is only strongly apparent at the lowest values of $\tilde{v}_a$ for which appreciable area fraction

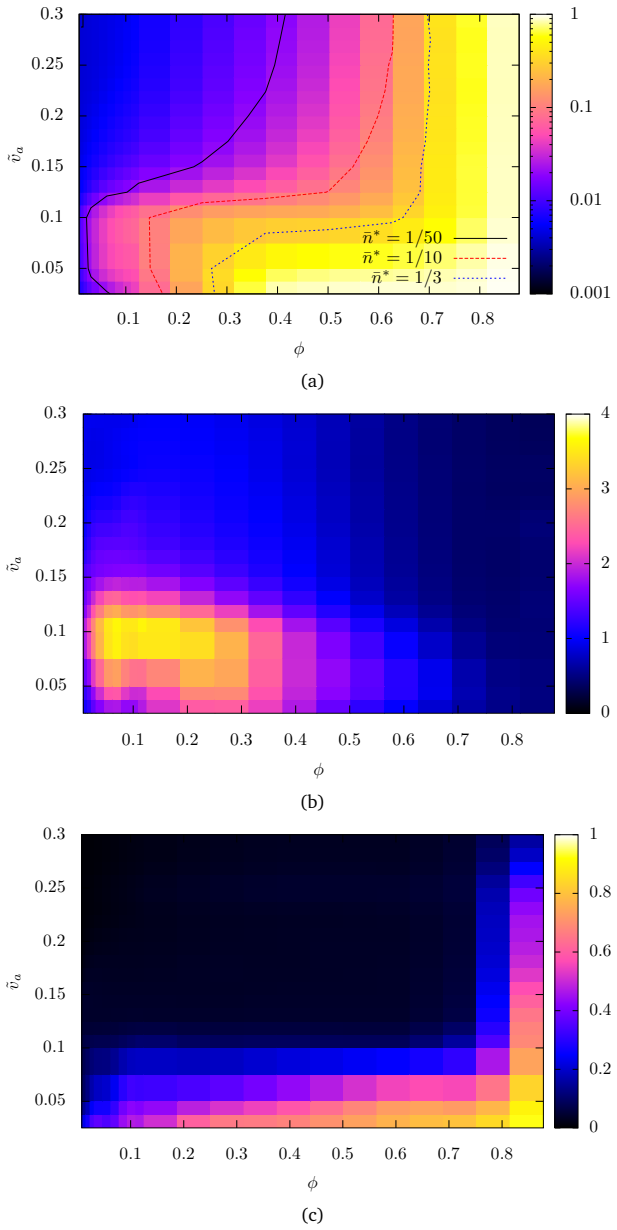

Fig. 11 Phase diagram of hydrodynamic squirmers mapped using (a) normalised mean number of particles per cluster $\bar{n}^* = \bar{n}/N$, (b) particle number fluctuations $\delta_N/\sqrt{\bar{N}}$ for $G = 5$ and c) hexatic order parameter Ψ_6.

fluctuations are present (Fig. 11b), reflecting the fact that the evidently phase separated snapshots in Fig. 10 only show solid-like ordering at the lowest v_a. In contrast, for the PBPs hexatic order (Fig. 4c) persists to higher values of $\tilde{D}$ relative to those for which appreciable phase separation is evident (Fig. 4b). The same is true of the column of hexatic ordering seen at high ϕ: this gradually fades with increasing $\tilde{v}_a$ in the squirmers, whereas it apparently persists to indefinitely high $\tilde{D}$ for the PBPs in Fig. 4c.

This gradual decay of hexatic order with increasing $\tilde{v}_a$ suggests that the attraction-dominated phase ordering is disrupted more readily by the ballistic intercollisional swimming of the squirmers with increasing $\tilde{v}_a$ than it is by the diffusive intercollisional dynamics of the PBP with increasing $\tilde{D}$. This is consistent with

the fact that these coherently moving "living crystals" seen in the regime of clustering at low $\tilde{v}_a$ in Fig. 10, are much more dynamic and mobile entities than their equilibrium counterparts in Fig. 3. The mean squared displacement (MSD) of particles in these clusters (data not shown) have an early-time ballistic regime crossing over into a later-time diffusive regime, even in crowded systems. In contrast, the counterpart MSDs for crowded PBPs at low $\tilde{D}$ have a slower-than-diffusive ("caged") regime at early times crossing over into diffusive dynamics later on (data not shown). Movies of these clusters can be found online[†] and are seen to resemble those observed experimentally in active colloids in Refs.[10,11,32], named as "living crystals".

Another notable difference is that stringlike clusters remain clearly evident in the squirmer snapshots even at high $\tilde{v}_a$ (Fig. 10), compared with the more complete return to homogeneity at high $\tilde{D}$ in the PBPs (Fig. 3). This is consistent with the existence of a larger window between the lines of $\bar{n}^* = 1/50$ and $1/10$ in Fig. 11a compared to its equilibrium counterpart in Fig. 4a, indicating a larger regime of clustering in the squirmers than in the PBPs. Likewise the area fraction fluctuations decay more slowly as a function of $\tilde{v}_a$ in Fig. 11 than they do as a function of $\tilde{D}$ in Fig. 4.

Clearly, this slight clustering of squirmers in the regime of high $\tilde{v}_a$ has no counterpart in the equilibrium phase diagram of the PBPs at high $\tilde{D}$. It is, however, reminiscent of the phase behaviour of ABPs for low to moderate values of ζ, where a slight clustering arises at high $\tilde{v}_a$, which we interpreted as a precursor to the onset of true MIPS at high ζ.

Tentatively, then, we interpret this tendency of the squirmers to form stringlike clusters at high $\tilde{v}_a$ as a counterpart of the slight clustering seen in the ABPs for modest imposed values of $\zeta = O(1)$. Recalling that ζ corresponds to the ratio of reorientation time and (estimated) collision time τ_o/τ_c that is imposed upfront in the ABP simulations, if this interpretation is correct we might then reasonably anticipate that the corresponding effective ratio $\zeta_{\text{eff}} \equiv \tau_o/\tau_c$ that *emerges* from the squirmer simulations should likewise be $O(1)$. This prediction of an emergent $\zeta = O(1)$ was indeed confirmed (for the case of hard disk squirmers) in Ref.[28]. It is furthermore consistent with earlier observations that whenever two squirmers scatter off each other hydrodynamically they also suffer an $O(1)$ change in their swim directions[29]. To reinforce this argument we extracted from our squirmer simulations this emergent effective ζ_{eff}, measuring the characteristic times τ_o and τ_c in the way defined in Ref.[28]. As can be seen in Fig. 12, we indeed recover $O(1)$ (or smaller) values for the effective emergent ζ_{eff} for all the mid-high area fractions, which would be the ones potentially inside the MIPS regime.

We therefore suggest that a slight tendency to clustering seen at high $\tilde{v}_a$ in the squirmers is the signature of a nearby MIPS, the full effects of which have been mitigated by the fact that the effective emergent value of ζ_{eff} for the squirmers is only $O(1)$, rather than the larger value of ζ needed to see full MIPS in the ABPs. The underlying physics here is that, as just noted, squirmers change their orientations each time they scatter off each other hydrodynamically, thereby giving an effective $\zeta_{\text{eff}} = O(1)$. In contrast for the ABPs we can artificially tune ζ to be arbitrarily large simply by setting a smaller D_r in the simulations, thereby inducing MIPS.

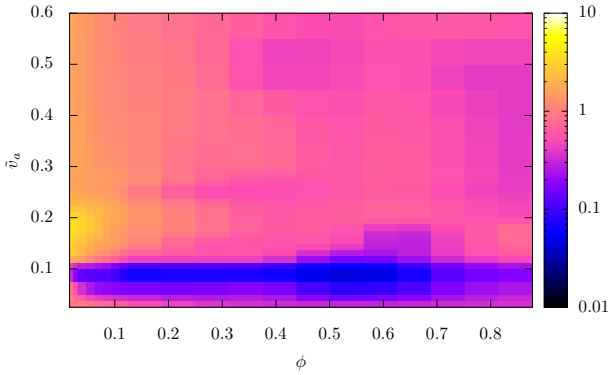

Fig. 12 Ratio between the characteristic reorientation time τ_o and collision time τ_c for polar squirmers, giving the emergent effective ratio ζ_{eff}.

As noted above, this suppression of MIPS by hydrodynamics was first discussed in the context of purely repulsive particles in Ref.[28]. A contribution of the present work has been to establish that MIPS is also suppressed by hydrodynamics in systems of attractive particles, despite any intuition one might have held upfront that attractive interactions might enhance the crowding mechanism of MIPS. The situation could however be different in systems such as in Janus particles[62] where the interaction potential is orientation-dependent and might be expected to increase the angular decorrelation time τ_o, thereby increasing the tendency towards MIPS.

Although we have demonstrated the suppression of MIPS by hydrodynamics only in this athermal limit of $D_r = 0$ and $D = 0$ for which we simulate the squirmers, it was in this limit that MIPS was found to be most pronounced in systems of ABPs without hydrodynamics in Ref.[27]. This gives a strong indication that MIPS should remain suppressed even at non-zero temperature, $D_r \neq 0$ and $D \neq 0$. Indeed, any extra thermal contribution to D_r would be expected only further to decrease the ratio of $\zeta_{\text{eff}} = \tau_o/\tau_c$, thereby further suppressing MIPS. The same argument would apply to the explicit inclusion of (athermal) tumbling events in the simulations.

To summarise, we suggest that the phase behaviour of attractive squirmers in the plane of $(\tilde{v}_a, \phi)$ can be understood in terms of two different mechanisms that smoothly blend into each other. The first is a regime of attraction-dominated phase separation at small $\tilde{v}_a$, which we suggest is analogous to the equilibrium phase separation seen in PBPs at small $\tilde{D}$, although more easily disturbed by the ballistic intercollisional dynamics of the squirmers as $\tilde{v}_a$ increases. The second is a regime of string-like particle clustering at high $\tilde{v}_a$, which we have interpreted in terms of a nearby MIPS that has been mitigated by the fact that $\zeta_{\text{eff}} = \tau_o/\tau_c$ is automatically $O(1)$ for squirmers, which reorient each time they scatter off each other.

So far, we have presented results for the hydrodynamic squirmers all for a single value of the stresslet parameter $\beta \equiv B_2/B_1 = 0.0$. We shall now briefly consider the effects on phase behaviour of varying β. Recall that a single particle in an infinite medium swims at a speed $v_a = B_1/2$, which is set only by B_1. The parameter B_2 instead measures an additional apolar contribution to the

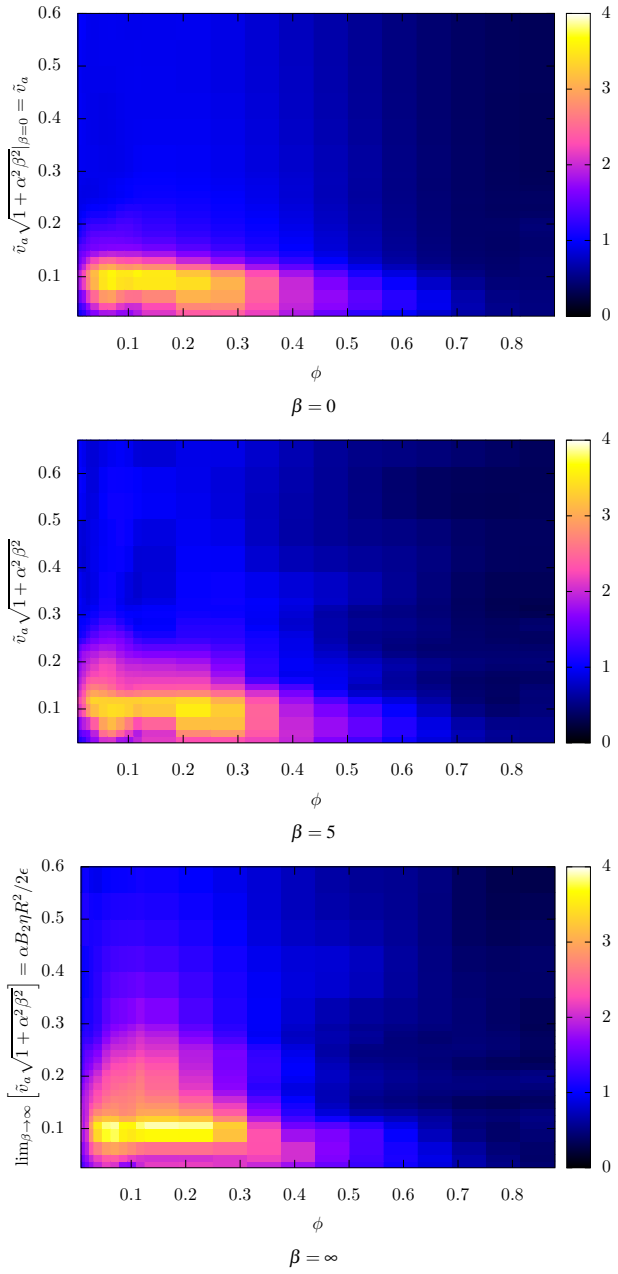

Fig. 13 Hydrodynamic squirmers. Area fraction fluctuations $\delta\phi$ obtained on dividing the simulation box into $G \times G$ subboxes with $G = 5$.

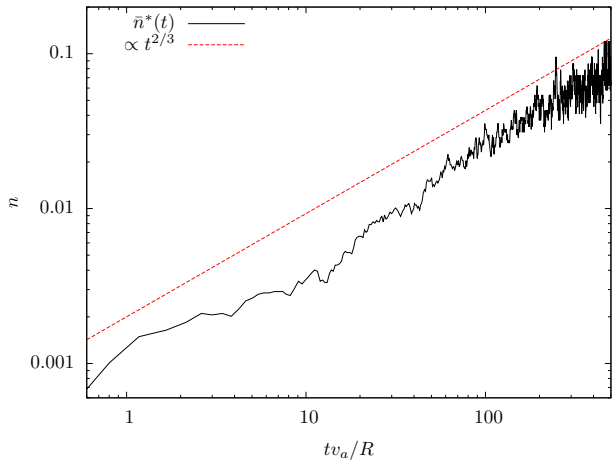

Fig. 14 Hydrodynamic squirmers, $\beta = 0.0$. Temporal evolution of the number of particles per cluster, $\bar{n}^*(t)$ (minus the initial contribution $\bar{n}^*(t=0)$). Time is shown in units of the characteristic time v_a/R that an isolated particle would take to displace one particle radius. The dotted line shows the power law $t^{2/3}$.

flow field that establishes round a (single, isolated) swimmer, and gives no contribution to the single-particle swim speed. In terms of the ratio $\beta = B_2/B_1$, therefore, the regime $|\beta| \ll 1$ corresponds to strongly polar swimmers while $|\beta| \gg 1$ corresponds to apolar "shakers".

Although B_2 has no effect on the swim speed of a single particle in an infinite medium, in the case of swimmers crowded together we might anticipate that the additional apolar flows governed by B_2 do lead to higher swim speeds for all the squirmers collectively, as the result of hydrodynamic interactions between them: the apolar contribution to the flow field round one squirmer disturbs neighbouring squirmers, causing them to move slightly faster.

In view of this, we suggest that the adimensionalised measure of activity $\tilde{v}_a$ on the vertical axis of the phase diagram should now be generalised from the bare quantity $\tilde{v}_a = B_1\eta R^2/2\varepsilon = v_a\eta R^2/\varepsilon$ used so far to a quantity that more fairly reflects the additional contribution of B_2 to the overall collective activity. Accordingly we combine B_1 and B_2 as $\sqrt{B_1^2+\alpha^2 B_2^2}$, and define an updated adimensional $\tilde{v}_a = v_a\sqrt{1+\alpha^2\beta^2}\eta R^2/\varepsilon$. (This reduces as required to the quantity $\tilde{v}_a = v_a\eta R^2/\varepsilon$ used to represent the $\beta = 0$ results above.) A key question then is whether the squirmers' phase behaviour in the plane of (this newly defined) $\tilde{v}_a$ and ϕ depends in any significant way on β.

The parameter α, which is defined by the formulae just given, deserves some discussion. In general it should depend on the area fraction ϕ, because the degree to which the apolar components of the flow field round each particle will cause neighbouring particles to move via hydrodynamic interactions will depend also on the particle separation and so on ϕ, consistent with the fact that B_2 has no effect on swimming dynamics in the single particle limit $\phi \to 0$, where only B_1 matters. However we shall ignore this complication in what follows and simply set α constant throughout.

Fig. 13 shows the phase behaviour of the squirmers, as measured by the particle number fluctuations, in this plane of $\tilde{v}_a = v_a\sqrt{1+\alpha^2\beta^2}\eta R^2/\varepsilon$ and ϕ for a value $\alpha = 0.1$. For this particular chosen value of α, the main features of the phase diagram are preserved in both magnitude and location even as β is varied between $0, 5, \infty$. Although all the panels shown in this figure are for pullers ($\beta > 0$), very similar results (not shown) are found for pushers ($\beta < 0$). Provided the data is represented in this way, we conclude that the stresslet parameter β is relatively unimportant in determining the clustering and phase behaviour of active particles with hydrodynamics, and that disklike "pushers", "pullers" and "shakers" should all show similar behaviour. The small value of α needed to ensure this – for other values the region of strong fluctuations shifts in vertical position with changing β – suggests that B_2 has a relatively large effect compared with B_1 in determining the overall magnitude of effective activity. This is consis-

tent with the notion that B_1 acts even in the limit of zero volume fraction whereas B_2 affects the activity levels through interactions only. Accordingly the effect of B_2 should scale as the inverse particle separation, which is large for the relatively crowded, clustered regimes of interest here.

Finally, we turn from the properties of the statistically steady state that forms a long time after the system was randomly initialised at time $t = 0$, to comment briefly on the dynamics of the aggregated domains that slowly coarsen at low v_a. See Fig. 14, which shows that the number of particles per domain $\bar{n}^*(t)$ appears to coarsen as a power law $t^{2/3}$, corresponding to a characteristic linear domain radius $t^{1/3}$, which we note is the same power law as for the coarsening dynamics of an undriven system in a diffusion dominated regime[60]. Given that the squirmers have hydrodynamic interactions and ballistic rather than diffusive intercollisional dynamics, this correspondence is a nontrivial and perhaps even surprising result.

7 Conclusions

Motivated by recent experiments reporting clustering in active suspensions[9–11,32], we have studied with full hydrodynamics the phase behaviour of active particles with an interaction potential that has an attractive Lennard-Jones (LJ) component, together with a steep repulsive contribution that diverges at particle contact $r \to 2R^+$, where R is the particle radius.

As a preliminary step we mapped out the equilibrium phase diagram of passive particles subject to the same interaction potential, finding phase behaviour broadly as expected for a LJ system, with regions of G-S, G-L and L-S phase coexistence at low temperatures. However compared to the LJ potential used more conventionally in the literature, the repulsive component of which diverges only as $r \to 0$, we found crystalline order to set in a slightly lower packing fractions, consistent with the greater excluded volume effects from the additional steeply repulsive contribution to our modified potential as $r \to 2R$. This preliminary study also established that the main features of phase behaviour can indeed be mapped out with only a small number of particles, $N = 242$, which is the maximum feasible system size in the much more costly hydrodynamic simulations.

As a second preliminary step, we then studied active Brownian particles (ABPs) subject to the same potential, but without hydrodynamics. As in previous studies of ABPs with the conventional Lennard-Jones potential[47], we observed two distinct regimes of phase separation. For low activities a regime of attraction-induced phase separation is seen, strikingly ressembling that at low temperatures in the equilibrium phase diagram, with a return to more homegeneous states for higher activities. In this sense, activity acts in a manner somewhat analogous to the temperature of a passive system. For ABPs with a small rotational diffusion coefficient, however, we found at high activities a second regime of phase separation that has no counterpart in the passive system and is instead a purely non-equilibrium phenomenon known as motility induced phase separation (MIPS)[21–23].

Motivated by the important effects of hydrodynamics in many active systems, we proceeded finally to simulate a suspension of hydrodynamic squirmers subject to the same (modified) LJ potential. The central results of this hydrodynamic study are fourfold.

First, we showed that activity again acts in a manner somewhat analogous to an effective temperature, in the sense that a regime of equilibrium-like attraction-induced phase separation is seen at low activities (with the activity suitably adimensionalised by the strength of the attractive potential), with a return to much more homogenised states at high activity.

Second, at high values of the (scaled) activity we find only weak stringlike clustering, with no evidence for motility induced phase separation (MIPS). By careful comparison with the ABPs, we interpreted this weak clustering as the signature of a nearby MIPS that has been largely suppressed by hydrodynamic interactions according to the arguments in Ref.[28].

In view of this suppression, we tentatively suggest that clustering phenomena seen experimentally in active colloids in which hydrodynamics is important are more likely to be in the regime of equilibrium-like attraction-dominated phase separation than the regime of purely non-equilibrium MIPS. Indeed, as noted above, the presence of a small phoretic attraction can seldom be ruled out in synthetic colloids. It is also interesting to recall that clustering is seldom seen in bacterial suspensions[33–35], at least in the absence of an obvious depletion interaction[36–38].

Third, we showed that the regime of phase separation seen at low activity, despite being broadly analogous to its equilibrium counterpart in the passive systems, also shows important differences. In particular we find a lower than expected degree of hexatic ordering, compared to the degree of clustering, consistent with the more dynamic nature of so these "living crystals"[10,11,32]. Activity is therefore seen to disrupt the level of translational ordering compared to that in the corresponding equilibrium phase diagram.

Fourth, we showed that an extended definition of the rescaled activity parameter allows us to recover strikingly similar phase diagrams across the full range of the stresslet parameter β, suggesting that "pushers", "pullers" and "shakers" all behave in a similar manner with regards their aggregation and phase behaviour.

In future work it would be interesting to consider more fully the consequences of dimensionality on these effects. Recall that the system simulated in this work concerns a 2D layer of active particles with 2D hydrodynamic interactions between them. While we are confident, on the basis of checks reported earlier in Ref.[28], that the same effects would also obtain for a 2D layer of particles with 3D hydrodynamic interactions, it would clearly be interesting to consider the case of 3D packings with 3D hydrodynamics. Indeed, loose aggregates moving coherently for long times were observed previously for a 3D suspension of purely repulsive squirmers with 3D hydrodynamics in Ref.[63]. In Ref.[61] a strongly confined 2D monolayer of purely repulsive squirmers was observed to show strong phase separation. However it should be noted that an important effect of strong confinement will be to screen hydrodynamic interactions. In this sense, therefore, the observation of strong phase separation in Ref.[61] is perhaps not surprising. Far more puzzlingly, phase separation was apparently observed in an unconfined 2D monolayer of purely repulsive squirmers with fully 3D hydrodynamics in Ref.[64], though at an area fraction $\phi = 0.1$ that seems far too low for MIPS to be

implicated.

Asymmetric particles could be considered in order to mimic chemotactic swimmers, with their rich phase diagrams[65–68]. A closer connection with experiments on phoretic active colloids might be established by solving the dynamics of a chemical concentration field in the fluid between the particles, with a suitable boundary condition at the particle surfaces, to account for diffusiophoresis.

Finally, in view of the important role played by the ratio ζ of the angular reorientation time to the interparticle collision time, it would be interesting to simulate elongated particles with full hydrodynamics. One might anticipate that particle elongation would significantly affect the angular reorientation time, perhaps leading to an effective emergent value of ζ, even with hydrodynamics, that would predispose a return to MIPS at high values of activity. It remains an open challenge to determine the link, if any, between that possible mechanism for MIPS in elongated particles and the one originally put forward in Refs.[15–20] in the context of active liquids crystals.

8 Acknowledgements

The research leading to these results has received funding from the European Research Council under the European Union's Seventh Framework Programme (FP7/2007-2013) / ERC grant agreement number 279365. The authors thank Mike Cates, Mark Miller, Ignacio Pagonabarraga and Francisco Alarcón for discussions.

References

1 F. Jülicher, K. Kruse, J. Prost, and J.-F. Joanny. Active behavior of the cytoskeleton *Physics Reports*, 449:3-28, 2007

2 M. Poujade, E. Grasland-Mongrain, A. Hertzog, J. Jouanneau, P. Chavrier, B. Ladoux, A. Buguin, and P. Silberzan. Collective migration of an epithelial monolayer in response to a model wound. *Proc. Nat. Acad. Sci. U.S.A.*, 104(41):15988-93, 2007.

3 H. C. Berg. E. coli in Motion *Springer*, New York, 2003.

4 S. Rafai, L. Jibuti, and P. Peyla. Effective viscosity of microswimmer suspensions. *Phys. Rev. Lett.*, 104:098102, 2010.

5 J. K. Parrish and W. M. Hamner. Three Dimensional Animal Groups. *Cambridge University Press*, Cambridge, England, 1997.

6 V. Narayan, S. Ramaswamy, and N. Menon. Long-lived giant number fluctuations in a swarming granular nematic. *Science*, 317(5834):105-8, 2007.

7 D. V. A. Kudrolli, G. Lumay and L. S. Tsimring. Swarming and Swirling in Self-Propelled Polar Granular Rods. *Phys. Rev. Lett.*, 100:058001, 2008.

8 J. Deseigne, O. Dauchot, and H. Chaté. Collective motion of vibrated polar disks. *Phys. Rev. Lett.*, 105:098001, 2010.

9 I. Theurkauff, C. Cottin-Bizonne, J. Palacci, C. Ybert, and L. Bocquet. Dynamic clustering in active colloidal suspensions with chemical signaling. *Phys. Rev. Lett.*, 108:268303, 2012.

10 Ivo Buttinoni, Julian Bialké, Felix Kümmel, Hartmut Löwen, Clemens Bechinger, and Thomas Speck. Dynamical clustering and phase separation in suspensions of self-propelled colloidal particles. *Phys. Rev. Lett.*, 110:238301, 2013.

11 F. Ginot, I. Theurkauff, D. Levis, C. Ybert, L. Bocquet, L. Berthier, and C. Cottin-Bizonne. Nonequilibrium Equation of State in Suspensions of Active Colloids. *Phys. Rev. X*,5:011004, 2015.

12 S. Ramaswamy. The mechanics and statistics of active matter. *Annual Review of Condensed Matter Physics*, 1(1):323–345, 2010.

13 M. C. Marchetti, J. F. Joanny, S. Ramaswamy, T. B. Liverpool, J. Prost, Madan Rao, and R. Aditi Simha. Hydrodynamics of soft active matter. *Rev. Mod. Phys.*, 85:1143–1189, 2013.

14 J. Bialké, T. Speck, and H. Löwen. Active colloidal suspensions: Clustering and phase behavior. *Journal of Non-Crystalline Solids*, (0):–, 2014.

15 J. Toner, and Y. Tu. Long-range order in a two-dimensional dynamical XY model: How birds fly together. *Phys. Rev. Lett.*, 75:4326–4329, 1995.

16 J. Toner, and Y. Tu. Flocks, herds, and schools: A quantitative theory of flocking. *Phys. Rev. E*, 58:4828–4858, 1998.

17 J. Toner, Y. Tu, and S. Ramaswamy. Hydrodynamics and phases of flocks. *Annals of Physics*, 318(1):170 – 244, 2005.

18 S. Ramaswamy, R. Aditi Simha, and J. Toner. Active nematics on a substrate: Giant number fluctuations and long-time tails. *EPL (Europhysics Letters)*, 62(2):196, 2003.

19 A. Baskaran, and M. C. Marchetti. Hydrodynamics of self-propelled hard rods. *Phys. Rev. E*, 77:011920, 2008.

20 A. Baskaran, and M. C. Marchetti. Enhanced diffusion and ordering of self-propelled rods. *Phys. Rev. Lett.*, 101:268101, 2008.

21 J. Tailleur, and M.E. Cates. Statistical mechanics of interacting run-and-tumble bacteria. *Physical review letters*, 100(21):218103, 2008.

22 M.E. Cates, D. Marenduzzo, I. Pagonabarraga, and J. Tailleur. Arrested phase separation in reproducing bacteria creates a generic route to pattern formation. *Proceedings of the National Academy of Sciences*, 107(26):11715–11720, 2010.

23 M. E. Cates, and J. Tailleur. Motility-Induced Phase Separation. *Annual Review of Condensed Matter Physics*, 6(1):219-244, 2015.

24 Y. Fily and M. C. Marchetti. Athermal phase separation of self-propelled particles with no alignment. *Phys. Rev. Lett.*, 108:235702, 2012.

25 Y. Fily, S. Henkes, and M. C. Marchetti. Freezing and phase separation of self-propelled disks. *Soft Matter*, 10:2132–2140, 2014.

26 J. Stenhammar, D. Marenduzzo, R. J. Allen, and M. E. Cates. Phase behaviour of active brownian particles: the role of dimensionality. *Soft Matter*, 10:1489–1499, 2014.

27 G. S. Redner, M. F. Hagan, and A. Baskaran. Structure and dynamics of a phase-separating active colloidal fluid. *Phys. Rev. Lett.*, 110:055701, 2013.

28 R. Matas-Navarro, R. Golestanian, T. B. Liverpool, and S. M. Fielding. Hydrodynamic suppression of phase separation in

active suspensions. *Phys. Rev. E*, 90:032304, 2014.

29 T. Ishikawa, M. P. Simmonds, and T. J. Pedley, Hydrodynamic interaction of two swimming microorganiems *Journal of Fluid Mechanics*, 568, 119-160, 2006.

30 D. Levis and L. Berthier. Clustering and heterogeneous dynamics in a kinetic monte carlo model of self-propelled hard disks. *Phys. Rev. E*, 89:062301, 2014.

31 J. Bialké, H. Löwen, and T. Speck. Microscopic theory for the phase separation of self-propelled repulsive disks. *EPL (Europhysics Letters)*, 103(3):30008, 2013.

32 J. Palacci, S. Sacanna, A. P. Steinberg, D. J. Pine, and P. M. Chaikin. Living crystals of light-activated colloidal surfers. *Science*, 339(6122):936–940, 2013.

33 A. Sokolov, I. S. Aranson, J. O. Kessler, and R. E. Goldstein. Concentration dependence of the collective dynamics of swimming bacteria. *Phys. Rev. Lett.*, 98:158102, 2007.

34 S. D Ryan, A. Sokolov, L. Berlyand, and I. S Aranson. Correlation properties of collective motion in bacterial suspensions. *New Journal of Physics*, 15(10):105021, 2013.

35 J. Dunkel, S. Heidenreich, K. Drescher, H. H. Wensink, M. Bär, and R. E. Goldstein. Fluid dynamics of bacterial turbulence. *Phys. Rev. Lett.*, 110:228102, 2013.

36 J. Schwarz-Linek, C. Valeriani, A. Cacciuto, M. E. Cates, D. Marenduzzo, A. N. Morozov, and W. C. K. Poon. Phase separation and rotor self-assembly in active particle suspensions. *Proceedings of the National Academy of Sciences*, 109(11):4052–4057, 2012.

37 J. Schwarz-Linek, A. Winkler, L. G. Wilson, N. T. Pham, T. Schilling, and W. C. K. Poon. Polymer-induced phase separation in escherichia coli suspensions. *Soft Matter*, 6:4540–4549, 2010.

38 G. Dorken, G. P. Ferguson, C. E. French, and W. C. K. Poon. Aggregation by depletion attraction in cultures of bacteria producing exopolysaccharide. *Journal of The Royal Society Interface*, 9(77):3490–3502, 2012.

39 Julian Bialké, Thomas Speck, and Hartmut Löwen. Crystallization in a Dense Suspension of Self-Propelled Particles. *Phys. Rev. Lett.*,108:168301, Apr 2012.

40 S. C. Takatori, W. Yan, and J. F. Brady . Swim Pressure: Stress Generation in Active Matter. *Phys. Rev. Lett.*, 113:028103, 2014.

41 L. Berthier. Nonequilibrium Glassy Dynamics of Self-Propelled Hard Disks. *Phys. Rev. Lett.*, 112:220602, 2014.

42 A. Wysocki, R. G. Winkler, and G. Gompper. Cooperative motion of active brownian spheres in three-dimensional dense suspensions. *EPL (Europhysics Letters)*, 105(4):48004, 2014.

43 R. Ni, M. A. Cohen Stuart, and M. Dijkstra. Pushing the glass transition towards random close packing using self-propelled hard spheres. *Nat Commun*, 4, 2013.

44 C. Reichhardt, and C. J. Olson Reichhardt. Absorbing phase transitions and dynamic freezing in running active matter systems. *Soft Matter*, 10:7502–7510, 2014.

45 R. Soto, and R. Golestanian. Run-and-tumble dynamics in a crowded environment: Persistent exclusion process for swimmers *Phys. Rev. E*, 89(1):012706, 2014.

46 B. M. Mognetti, A. Šarić, S. Angioletti-Uberti, A. Cacciuto, C. Valeriani, and D. Frenkel. Living clusters and crystals from low-density suspensions of active colloids. *Phys. Rev. Lett.*, 111:245702, 2013.

47 G. S. Redner, A. Baskaran, and M. F. Hagan. Reentrant phase behavior in active colloids with attraction. *Phys. Rev. E*, 88:012305, 2013.

48 P. Vasileios, S. Harmen, and F. Laura. Self-assembly of active attractive spheres. *S*oft Matter, 11:4158, 2015.

49 M. J. Lighthill. On the squirming motion of nearly spherical deformable bodies through liquids at very small reynolds numbers. *Communications on Pure and Applied Mathematics*, 5(2):109–118, 1952.

50 J. R. Blake. A spherical envelope approach to ciliary propulsion. *Journal of Fluid Mechanics*, 46(01):199–208, 1971.

51 M. Rovere, D. W. Heermann, and K. Binder. The gas-liquid transition of the two-dimensional Lennard-Jones fluid. *Journal of Physics: Condensed Matter*, 2(33):7009, 1990.

52 J.-P. Hansen and L. Verlet. Phase transitions of the lennard-jones system. *Phys. Rev.*, 184:151–161, 1969.

53 B. J. Alder, and T. E. Wainwright. Studies in Molecular Dynamics. II. Behavior of a Small Number of Elastic Spheres. *The Journal of Chemical Physics* 33(5):1439-1451,1960.

54 J. R. Blake. Self propulsion due to oscillations on the surface of a cylinder at low Reynolds number. *Bull. Austr. Math. Soc.*, 5(2):255–264, 1971.

55 T. Ishikawa, J. T. Locsei, and T. J. Pedley. Development of coherent structures in concentrated suspensions of swimming model micro-organisms. *Journal of Fluid Mechanics*, 615:401–431, 11 2008.

56 A. K. Jain, M. N. Murty, and P. J. Flynn. Data clustering: A review. *ACM Comput. Surv.*, 31(3):264–323, 1999.

57 S.C. Johnson. Hierarchical clustering schemes. *Psychometrika*, 32(3):241-254, 1967.

58 Z. Wang, A. M. Alsayed, A. G. Yodh, and Y. Han. Two-dimensional freezing criteria for crystallizing colloidal monolayers. *The Journal of Chemical Physics*, 132(15):–, 2010.

59 J. Tang, G. Ge, and L. E. Brus. Gasliquidsolid phase transition model for two-dimensional nanocrystal self-assembly on graphite. *The Journal of Physical Chemistry B*, 106(22):5653–5658, 2002.

60 P. Chaikin, T. C. Lubensky. Principles of condensed matter physics. *Cambridge University Press*, Cambridge, England, 1995.

61 A. Zöttl and H. Stark. Hydrodynamics determines collective motion and phase behavior of active colloids in quasi-two-dimensional confinement. *Phys. Rev. Lett.*, 112:118101, 2014.

62 T. Bickel, G. Zecua, and A. Würger. Polarization of active janus particles. *Phys. Rev. E*, 89:050303, 2014.

63 F. Alarcón and I. Pagonabarraga. Spontaneous aggregation and global polar ordering in squirmer suspensions. *Journal of Molecular Liquids*, 185(0):56 – 61, 2013.

64 T. Ishikawa and T. J. Pedley. Coherent structures in mono-

layers of swimming particles. *Phys. Rev. Lett.*, 100:088103, 2008.

65 R. Golestanian, T. B. Liverpool, and A. Ajdari. Designing phoretic micro- and nano-swimmers. *New Journal of Physics*, 9(5):126, 2007.

66 S. Saha, R. Golestanian, and S. Ramaswamy. Clusters, asters, and collective oscillations in chemotactic colloids. *Phys. Rev. E*, 89(6):062316, 2014.

67 R. Soto, and R. Golestanian. Self-Assembly of Catalytically Active Colloidal Molecules: Tailoring Activity Through Surface Chemistry. *Phys. Rev. Lett.*, 112(6):068301, 2014.

68 M. Yang, A. Wysocki, and M. Ripoll. Hydrodynamic simulations of self-phoretic microswimmers. *Soft Matter*, 10(33):6208-6218, 2140.